Inorg. Chem. **2003**, *42*, 5974–5988

Density Functional Study of the Electric Hyperfine Interactions and the Redox-Structural Correlations in the Cofactor of Nitrogenase. Analysis of General Trends in ^{57}Fe Isomer Shifts

Vladislav Vrajmasu, Eckard MUnck,* and Emile L. Bominaar*

Department of Chemistry, Carnegie Mellon University, 4400 Fifth Avenue, Pittsburgh, Pennsylvania 15213

Received April 25, 2003

The influence of the interstitial atom, X, discovered in a recent crystallographic study of the MoFe protein of nitrogenase, on the electric hyperfine interactions of ^{57}Fe has been investigated with density functional theory. A semiempirical theory for the isomer shift, δ, is formulated and applied to the cofactor. The values of δ for the relevant redox states of the cofactor are predicted to be higher in the presence of X than in its absence. The analysis strongly suggests a [$Mo^{4+}4Fe^{2+}3Fe^{3+}$] oxidation state for the $S = {}^3/_2$ state M^N. Among C^{4-}, N^{3-}, and O^{2-}, oxide is found to be the least likely candidate for X. The analysis suggests that X should be present in the cofactor states M^{OX} and M^R as well as in the alternative nitrogenases. The calculations of the electric field gradients (EFGs) indicate that the small values for ΔE_Q in M^N result from an extensive cancellation between valence and ligand contributions. X emerges from the analysis of the hyperfine interactions as an ionically bonded species. Its major effect is on the asymmetry parameters for the EFGs at the six equatorial sites, Fe_{Eq}. A spin-coupling scheme is proposed for the state [$Mo^{4+}4Fe^{2+}3Fe^{3+}$] that is consistent with the measured ^{57}Fe **A**-tensors and ΔE_Q values for M^N and identifies the unique site exhibiting the small **A** value with the terminal Fe site, Fe_T. The optimized structure of a cofactor model has been calculated for several oxidation states. The study reveals a contraction in the average Fe–Fe distance upon increasing the number of electrons stored in the cluster, in accord with extended X-ray absorption fine structure studies. The reliability of the adopted methodology for predicting redox-structural correlations is tested for cuboidal [4Fe–4S] clusters. The calculations reveal a systematic increase in the S···S sulfide distances, in quantitative agreement with the available data. These trends are rationalized by a simple electrostatic model.

1. Introduction

The discovery of an interstitial, non-sulfur atom, X, in the 1.16-Å resolution structure of the catalytically essential Fe−Mo cofactor (FeMoco, M center) in the iron−molybdenum protein of nitrogenase by Rees and co-workers[1] raises a number of questions: What element is X? Is X only present in the $S = {}^3/_2$ state M^N, or is it retained in the other known redox states, M^{OX} and M^R? Do the all-iron and vanadium−iron cofactors in the alternative nitrogenases contain a central atom as well? How does X influence the structure of the cofactor? Does the presence of X preclude certain substrate binding conformations and protonation states? What is the effect of X on the hyperfine parameters of the seven Fe sites in the cofactor? Does the presence of the interstitial atom change any of the earlier conclusions concerning the cofactor oxidation state that were based, at least in part, on the X-free structure? We have addressed some of these questions by performing density functional theory (DFT) calculations on a model for the cofactor cluster. These efforts focus on the electric hyperfine parameters, notably the site-averaged value for the isomer shift, δ_{av}, for which accurate data are available in the states M^N, M^{OX}, and M^R. Münck and co-workers[2] have analyzed δ_{av} for assessing the formal oxidation state of M^N, using an interpolation between estimates for the isomer shifts of ferrous and ferric trigonal sites. Given that the electron count is odd for the $S = {}^3/_2$ state of M^N and relying on the ENDOR information,[3] which suggests that the molybdenum site is Mo^{4+}, the most relevant formal oxidation states to be

* Authors to whom correspondence should be addressed. E-mail: em40@andrew.cmu.edu (E.M.); eb7g@andrew.cmu.edu (E.L.B.).

(1) Einsle, O.; Tezcan, F. A.; Andrade, S. L. A.; Schmid, B.; Yoshida, M.; Howard, J. B.; Rees, D. C. *Science* **2002**, *297*, 1696.

(2) Yoo, S. J.; Angove, H. C.; Papaefthymiou, V.; Burgess, B. K.; Münck, E. *J. Am. Chem. Soc.* **2000**, *122*, 4926.

10.1021/ic0301371 CCC: $25.00
Published on Web 08/26/2003

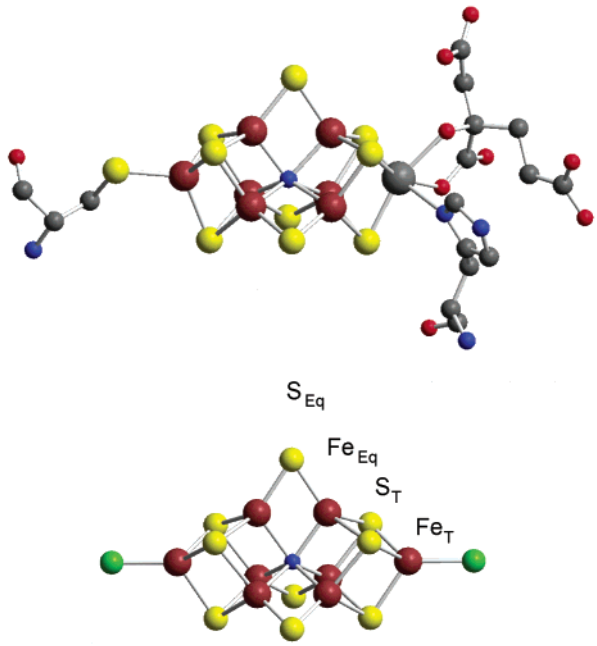

Figure 1. (Top) FeMoco in crystallographic structure of the iron−molybdenum protein from *A. vinelandii*, revealing an interstitial atom, X (ref 1). (Bottom) Model used in calculations together with atom labeling used in text. T stands for terminal and Eq for equatorial. Irons in notations $Fe_{Eq}-Fe_{Eq}$ and $Fe_{Eq}-Fe_{Eq'}$ belong to different and same cuboidal moieties, respectively. Colors: brown (Fe), yellow (S), blue (N or X), gray and big (Mo), gray and small (C), red (O), and green (Cl).

considered are $[Mo^{4+}6Fe^{2+}1Fe^{3+}]$ and $[Mo^{4+}4Fe^{2+}3Fe^{3+}]$. On the basis of $\delta = 0.57$ mm s^{-1}, obtained from Mössbauer studies of Power's complex[4,5] $[Fe^{2+}(SC_6H_3(t\text{-}Bu)_2)_3]^-$, as an estimate for the isomer shift of ferrous equatorial cofactor irons (Figure 1), and the drop in δ by 0.45 mm s^{-1}, as typically observed for FeS_4 sites when passing from ferrous to ferric, the average cofactor isomer shift, $\delta_{av} = 0.41$ mm s^{-1}, could only arise from oxidation state $[Mo^{4+}4Fe^{2+}3Fe^{3+}]$. However, the analysis presented below indicates that the δ values of the three-coordinate thiolate sites are overestimates of the corresponding quantities of the equatorial cofactor sites. The alternative oxidation state, $[Mo^{4+}6Fe^{2+}1Fe^{3+}]$, was proposed by Noodleman and collaborators[6] from DFT analysis of Mössbauer isomer shifts, albeit without consideration of interstitial atom X, and by Hoffman and coworkers,[3] based on ENDOR of the $S = {}^1/_2$, CO-bound form of M^N. However, the magnetic hyperfine tensors, **A**, obtained from ENDOR for the spin-coupled $S = {}^3/_2$ state depend on a large number of unknowns, viz., the intrinsic **A**-values and spin projection factors for the individual iron sites. Hence, conclusions concerning the oxidation state can only be drawn from these data by making detailed assumptions about the electronic structure of the cofactor. Taking into consideration the different topologies, it is questionable whether presumed features such as spin-ordered, delocalized-mixed-valence pairs, which are the hallmark of iron−sulfur cubanes, also exist in the cofactor. To avoid the complexities arising from spin ordering and valence delocalization, we present an approach toward determining the oxidation state of M^N that rests on an analysis of the site-averaged isomer shift of the cofactor in the ferromagnetic, spin-ordered, state. An explanation is given for the remarkably small quadrupole splittings observed in the state M^N. Finally, we have calculated the cofactor structure for various oxidation states and found a contraction in the average Fe−Fe distance upon reduction, in agreement with the extended X-ray absorption fine structure (EXAFS) measurements on M^N and M^{OX} reported by Christiansen et al.[7] The contraction mechanism is discussed and tested against the structure data for cuboidal iron−sulfur clusters.

2. Materials and Methods

2.1. Density Functional Theory. Density functional calculations were performed, using Becke's three-parameter hybrid functional (B3LYP) provided by the Gaussian98 software package.[8] The density functional B3LYP was selected because of its excellent performance in previous studies of ^{57}Fe isomer shifts.[9,10] For reasons of computational economy and comparability, we restricted ourselves in this study to the use of standard basis sets. The geometry optimizations conducted here employed the all-electron basis set 6-311G. This basis provides for efficient geometry optimizations of good quality[11−19] and can be applied to large clusters, such as the cofactor model, without exceeding the temporal limits of our computational facilities.[20] The optimizations were terminated when the default convergence criterion was met.[8] The stabilities of the optimized geometries were verified by performing frequency calculations, and the final structures were checked against the available X-ray and neutron-diffraction data. Subsequently, all electron wave functions were evaluated by single point calculations for the optimized structures with the basis 6-311G (with or without

(3) Lee, H.-I.; Hales, B. J.; Hoffman, B. M. *J. Am. Chem. Soc.* **1997**, *119*, 11395.
(4) Sanakis, Y.; Power, P. P.; Stubna, A.; Münck, E. *Inorg. Chem.* **2002**, *41*, 2690.
(5) MacDonnell, F. M.; Ruhlandt-Senge, K.; Ellison, J. J.; Holm, R. H.; Power, P. P. *Inorg. Chem.* **1995**, *34*, 1815.
(6) Lovell, T.; Li, J.; Liu, T.; Case, D. A.; Noodleman, L. *J. Am. Chem. Soc.* **2001**, *123*, 12392.
(7) Christiansen, J.; Tittsworth, R. C.; Hales, B. J.; Cramer, S. P. *J. Am. Chem. Soc.* **1995**, *117*, 10017.
(8) Frisch, M. J.; Trucks, G. W.; Schlegel, H. B.; Scuseria, G. E.; Robb, M. A.; Cheeseman, J. R.; Zakrzewski, V. G.; Montgomery, J. A., Jr.; Stratmann, R. E.; Burant, J. C.; Dapprich, S.; Millam, J. M.; Daniels, A. D.; Kudin, K. N.; Strain, M. C.; Farkas, O.; Tomasi, J.; Barone, V.; Cossi, M.; Cammi, R.; Mennucci, B.; Pomelli, C.; Adamo, C.; Clifford, S.; Ochterski, J.; Petersson, G. A.; Ayala, P. Y.; Cui, Q.; Morokuma, K.; Malick, D. K.; Rabuck, A. D.; Raghavachari, K.; Foresman, J. B.; Cioslowski, J.; Ortiz, J. V.; Stefanov, B. B.; Liu, G.; Liashenko, A.; Piskorz, P.; Komaromi, I.; Gomperts, R.; Martin, R. L.; Fox, D. J.; Keith, T.; Al-Laham, M. A.; Peng, C. Y.; Nanayakkara, A.; Gonzalez, C.; Challacombe, M.; Gill, P. M. W.; Johnson, B. G.; Chen, W.; Wong, M. W.; Andres, J. L.; Head-Gordon, M.; Replogle, E. S.; Pople, J. A. *Gaussian 98*, revision A.11; Gaussian, Inc.: Pittsburgh, PA, 1998.
(9) Neese, F. *Inorg. Chim. Acta* **2002**, *337*, 181.
(10) Zhang, Y.; Mao, J.; Oldfield, E. *J. Am. Chem. Soc.* **2002**, *124*, 7829.
(11) Krishnan, R.; Binkley, J. S.; Seeger, R.; Pople, J. A. *J. Chem. Phys.* **1980**, *72*, 650.
(12) Wachters, A. J. H. *J. Chem. Phys.* **1970**, *52*, 1033.
(13) Dewar, M. J. S.; Reynolds, C. H. *J. Comput. Chem.* **1986**, *7*, 140.
(14) McLean, A. D.; Chandler, G. S. *J. Chem. Phys.* **1980**, *72*, 5639.
(15) Raghavachari, K.; Pople, J. A.; Replogle, E. S.; Head-Gordon, M. *J. Phys. Chem.* **1990**, *94*, 5579.
(16) Hay, P. J. *J. Chem. Phys.* **1977**, *66*, 4377.
(17) Binning, R. C., Jr.; Curtiss, L. A. *J. Comput. Chem.* **1990**, *11*, 1206.
(18) Curtiss, L. A.; McGrath, M. P.; Blaudeau, J.-P.; Davis, N. E.; Binning, R. C., Jr.; Radom, L. *J. Chem. Phys.* **1995**, *103*, 6104.
(19) McGrath, M. P.; Radom, L. *J. Chem. Phys.* **1991**, *94*, 511.
(20) Computations were performed on 2-nodes Athlon MP 2000+ and 2100+ workstations. Typical computational times were up to 6 h for a single point calculation and up to 48 h for a geometry optimization.

addition of polarized and/or diffuse functions and the Wachters (+f) basis[12]). The stability of the ground state was checked by performing time-dependent DFT calculations, and the orbital populations were altered until all monoelectronic excitation energies were positive. These calculations were guided by Mulliken population analyses of the electron distributions. A locally developed program (MOPOP) was implemented to facilitate the population analysis of polynuclear transition-metal complexes. The program extracts data from the formatted checkpoint and output files of DFT jobs as input for calculating the electronic population per atom and per atom type in molecular orbitals of choice. The information thus obtainable provided an indispensable guidance in the search for the proper ground state among the large number of close-lying states of the cofactor model. The self-consistent field (SCF) iterations were terminated upon reaching tight convergence criteria (10^{-6} root-mean-square deviation in the density matrix and 10^{-8} au maximum deviation in energy).

2.2. Electron Density and Quadrupole Splitting. The electron density at the iron nucleus was computed by the program DELTA that we developed for this purpose and for analyzing contributions to the density from subsets of molecular orbitals specified by the user. Electric field gradients (EFG) at the iron nuclei, computed with the properties package of Gaussian98, were used to predict the quadrupole splittings, ΔE_Q, $\Delta E_Q = (1/2)eQV_{zz}(1 + (1/3)\eta^2)^{1/2}$, which were judged against the experimental values for this observable to validate the quality of the DFT solutions. The expression for ΔE_Q depends on the positive unit charge (e), the nuclear quadrupole moment in the excited $I = {}^3/_2$ state of the ^{57}Fe nucleus (Q), and the asymmetry parameter $\eta = (V_{xx} - V_{yy})/V_{zz}$, where the V_{ii} are principal components of the sign-reversed EFG tensor. The Q of ^{57}Fe was treated as an adjustable parameter for matching the computational results to the experimental values for ΔE_Q in a large set of iron complexes. The best overall agreement was obtained by taking $Q = 0.15$ b (6-311G) and $Q = 0.16$ b[21] (6-311+G* and Wachters (+f)).

2.3. Isomer Shift Calibration. Classical electrostatics predict that the isomer shift (δ) is a linear function of the electron density at the ^{57}Fe nucleus, $\rho(0)$, i.e., $\delta = \alpha(\rho(0) - C) + \delta_0$, where α is a constant depending on the change in the distribution of the nuclear charge upon γ absorption and $(-\alpha C + \delta_0)$ is a parameter chosen to conform to the particular standard material (typically Fe metal) used for defining the origin of the Doppler-velocity energy scale and C is set to 11 617 e^-/a_0^3. A number of small mononuclear iron compounds with δ values unaffected by solid-state effects, hydrogen bonding, steric repulsions, or close (pseudocoordinative) contacts and which cover the full range of ^{57}Fe shifts were selected for calibrating the relationship between the experimental isomer shifts, δ_{exp}, and the calculated electron densities at iron nuclei, $\rho_{calc}(0)$ (Supporting Information (SI) Figure S.1). The calibration process consisted of three steps. First, the geometries of the complexes in the calibration set were optimized at the B3LYP/LanL2DZ level of theory, using symmetrized structures obtained by averaging X-ray data as a starting point. Second, the LanL2DZ-based geometries were used as a starting point for subsequent geometry optimizations using the 6-311G basis set. The structures optimized at the B3LYP/6-311G level were used to compute electron densities at the ^{57}Fe nuclei in the calibration complexes, $\rho_{calc}(0)$. Third, the $\rho_{calc}(0)$ values were plotted vs the experimental isomer shifts (δ_{exp}), and the resulting graph was subjected to a linear regression analysis. In the third step it is essential to convert all isomer shifts to the same standard and temperature. The experimental isomer shifts reported in this work are quoted with respect to α-Fe at room temperature and refer to a sample temperature of 4.2 K. In cases where 4.2-K data were lacking, the isomer shifts were obtained by extrapolating high-temperature data to correct for second-order Doppler shift (SOD). The SOD is almost zero at temperatures below ~70 K and decreases roughly linearly beyond this temperature with slope $d\delta_{SOD}/dT = -5 \times 10^{-4}$ mm s^{-1}/K. Accordingly, the isomer shift data recorded above 70 K were converted to the 4.2-K value, $\delta(4.2\text{ K}) = \delta(T) - (T - 70\text{ K})\, d\delta_{SOD}/dT$. The regression analysis yields correlation coefficient $R = 0.998$ and calibration constants $\alpha = -0.322 \pm 0.009$ mm s^{-1}/a_0^{-3} and $\delta_0 = 0.08 \pm 0.01$ mm s^{-1}. The correlation is excellent and allows us to predict the isomer shift with a precision of ± 0.04 mm s^{-1} at the 68% probability level. Among the basis sets tested, the calibration procedure results in the best correlation for the basis 6-311G.

2.4. Calculations for Cofactor Models. The geometry for the cofactor model was designed to yield a realistic system with the highest possible symmetry, i.e., D_{3h}. This objective was achieved by substituting Mo with Fe[22] and the terminal residues with one chloride at each extreme of the cluster and by averaging over the equivalent atom positions in the recently published structure,[1] conferring mirror symmetry along the plane containing the three equatorial sulfur atoms and the heteroatom. The resulting cofactor models (see Figure 1) have the formulations $[Fe_8XS_9Cl_2]^n$, X = Ø, O, N, and C, where n is the total charge of the cluster, which is the sum of the formal charges in the conventional oxidation states for the atoms (S^{2-}, $Fe^{2+/3+}$, Cl^-, O^{2-}, N^{3-}, and C^{4-}). The optimized geometries, electronic structures, and isomer shifts of the polynuclear model compounds were computed for states in which the iron spins were ferromagnetically ordered (see Discussion). We performed a sequence of DFT calculations for models with different entries for X and n. The first calculations were performed for the model with eight Fe^{3+} ions ($n = +2$) and oxygen as the central atom (X = O). The final solution of the latter computations was taken as the starting point for calculating the electronic structures and optimized geometries for the two-electron-reduced cluster state. A similar procedure was adopted in the subsequent reduction steps, leading to the computational sequence $8Fe^{3+} \rightarrow 6Fe^{3+}/2Fe^{2+} \rightarrow 4Fe^{3+}/4Fe^{2+} \rightarrow 2Fe^{3+}/6Fe^{2+}$. No satisfactory solutions were obtained for the fully reduced cluster, $[8Fe^{2+}]$. The calculations for the systems with alternative central atoms were performed in the order O → N → C and took advantage of the results from the preceding runs. Finally, the isomer shifts were calculated for the optimized structures and, for the sake of comparison, also for the X-ray-averaged structure.

2.5. Isomer Shifts for Cofactor. To ensure a consistent application of the proposed semiempirical theory for the isomer shift, the same procedure as the one used for calculating the electron densities in the calibration set was applied to evaluating the densities at the iron nuclei in the cofactor. Thus, the isomer shifts were computed at the B3LYP/6-311G level for geometries that were optimized with the same (6-311G) basis set. Since the calibration constants for the isomer shift depend on the choices for the basis sets in the first two steps of the calibration process (the value for α can differ by as much as a factor of 2, depending on the methodology used for calculating the electron density),[6,9,10,23] the constants derived from structures obtained with larger bases cannot be used for converting electron densities from 6-311G structures

(21) Havlin, R. H.; Godbout, N.; Salzmann, R.; Wojdelski, M.; Arnold, W.; Schulz, C. E.; Oldfield, E. *J. Am. Chem. Soc.* **1998**, *120*, 3144.

(22) Siegbahn, P. E. M.; Westerberg, J.; Svensson, M.; Crabtree, R. H. *J. Phys. Chem. B* **1998**, *102*, 1615.

(23) Lovell, T.; Torres, R. A.; Han, W.-G.; Liu, T.; Case, D. A.; Noodleman, L. *Inorg. Chem.* **2002**, *41*, 5744.

into isomer shifts. Like in any other case of semiempirical theory, a consistent use of parameterization is essential.

3. Results and Discussion

3.1. Hyperfine Parameters and Oxidation State Assignments for Cofactor. 3.1.1. Calibration of Isomer Shift. DFT has been of great utility in describing the ground-state properties of molecular systems. It has been shown, for example, that computation of electric field gradients with hybrid functionals and accurate basis sets centered on the atoms in the first coordination sphere can be utilized to predict the quadrupole splittings observed with Mössbauer spectroscopy.[21] In 2002, several authors[9,10,23] reported high-quality correlations between the computed electron densities on ^{57}Fe nuclei and the observed isomer shifts. Theory predicts that the relationship between the aforementioned quantities is linear.[24] The critical outcome parameter of the calibration is the standard deviation that determines the accuracy and applicability of the isomer shifts prediction/correlation. Published calibrations yield standard deviations of about 0.1 mm s^{-1}, a value that can serve as a good indicator of the oxidation and spin states for mononuclear iron complexes.[9,10,23] However, the applicability of such calibrations for distinguishing between coordination numbers and partial oxidation states in polynuclear clusters is limited to cases where changes in δ are large. It is well-established that the bulk of the electron density at the ^{57}Fe nucleus is provided by the 1s and 2s population, but the relevant changes occur due to changes in 3s and 4s densities at the nucleus.[25] Changes in δ in going from one oxidation state to another are driven mainly by electronic and geometric relaxations.[9] While the electronic relaxation is typically well accounted for in calculations, the geometric relaxation depends on the choice of the basis set and the model for the molecular system. Available structure data for iron compounds suffer from small random errors due to limitations in resolution and from systematic errors from thermal averaging over vibrations.[26−32] Inaccuracies in the bond lengths computed by DFT geometry optimizations are an additional cause of discrepancy between theory and experiment. However, systematic errors can be minimized by proper calibration, leaving random errors as the main source of the standard deviation. Our calibration curve spans a δ range of ~2 mm s^{-1} and provides a reliable estimate for α and a consistent value of $(-\alpha C + \delta_0)$. As mentioned in Materials and Methods, we have carefully chosen compounds which are free from H bonding, solid-state effects, steric repulsions, and close (pseudocoordinative) contacts as these interactions may affect the bond lengths. The accompanying changes in δ have their origin in high dδ/dR values. To corroborate this point we will discuss the isomer shift for the trigonal complex $[Fe(SR)_3]^-$, where R = $C_6H_2(t\text{-}Bu)_3$. Of course, one can improve the semiempirical method for predicting δ values by computing geometries with higher accuracy basis sets. For example, the standard deviation computed for the same calibration set of compounds, but obtained with optimized geometries for Wachters (+) set on iron and 6-311G on the ligand atoms, improves from 0.04 to 0.03 mm s^{-1} when the electronic densities at the iron nuclei are computed with the 6-311G basis set.[33,34]

Table 1. Distance Dependence of Isomer Shift, δ

complex	structure	R_{opt} (Å)	δ (mm s^{-1})	dδ/dR (mm s^{-1}/Å)
$[Fe^{3+}Cl_3]^0$	trigonal planar	2.179	0.344	0.84
$[Fe^{2+}Cl_3]^{1-}$	trigonal planar	2.288	0.667	0.84
$[Fe^{3+}Cl_4]^{1-}$	tetrahedral	2.266	0.387	0.71
$[Fe^{2+}Cl_4]^{2-}$	tetrahedral	2.448	0.966	0.37
$[Fe^{3+}F_3]^0$	trigonal planar	1.684	0.234	2.12
$[Fe^{3+}F_4]^{1-}$	tetrahedral	1.826	0.431	0.86
$[Fe^{3+}F_6]^{3-}$	octahedral	2.006	0.537	0.58

3.1.2. Qualitative Trends of the Isomer Shift. To gain insight in the factors that influence δ, we have calculated this quantity for a number of small model complexes. Some of the results are summarized in Table 1. There are three major contributions to the variations in isomer shift: (a) Addition of electrons to an iron center that is coordinated to a fixed number of ligands placed at constant distances from the metal increases δ, $\Delta\delta_{redox} > 0$, because a higher 3d population enhances the shielding of the attractive interaction between the s electrons and iron nucleus, decreases $\rho(0)$, and thus increases δ. (b) An increase of the distances of a fixed number of ligands to an iron site that maintains its oxidation and spin states increases δ, $\Delta\delta_{distance} > 0$, because larger Fe−ligand distances entail less electron donation to the metal 4s orbital, thus diminishing $\rho(0)$ and increasing δ. (c) An increase in the number of ligands, N, while keeping the same iron−ligand distances, metal oxidation, and spin states, decreases δ, $\Delta\delta_{coord} < 0$, because an increase in N increases electron donation to the 4s iron orbital, increasing $\rho(0)$ and thus decreasing δ. Rules (b) and (c) indicate that changes in 4s population outweigh those of changes 3d shielding. In the use of these qualitative rules, it should be borne in mind that (electro)chemical modifications may give rise to either equally or oppositely signed contributions to δ. For example, an increase in coordination number ($\Delta\delta_{coord} < 0$) leads to a weakening and lengthening of the individual iron−ligand bonds and to an additional contribution of opposite sign

(24) Gütlich, P.; Link, R.; Trautwein, A. *Mössbauer Spectroscopy and Transition Metal Chemistry*; Springer-Verlag: New York, 1978.
(25) Freeman, A. J.; Ellis, D. E. In *Mössbauer Isomer Shifts*; Shenoy, G. K., Wagner, F. E., Eds.; North Holland Pub. Co.: New York, **1978**, p 111.
(26) Cruickshank, D. W. J. *Acta Crystallogr.* **1956**, *9*, 757.
(27) Cruickshank, D. W. J. *Acta Crystallogr.* **1961**, *14*, 896.
(28) Busing, W. R.; Levy, H. A. *Acta Crystallogr.* **1964**, *17*, 142.
(29) Pawley, G. S. *Acta Crystallogr., Sect. B*: *Struct. Crystallogr. Cryst. Chem.* **1968**, *24*, 485.
(30) Johnson, C. K. *Crystallogr. Comput., Proc. Int. Summer Sch.* **1970**, 220.
(31) Schomaker, V.; Trueblood, K. N. *Acta Crystallogr., Sect. B*: *Struct. Crystallogr. Cryst. Chem.* **1968**, *24*, 63.
(32) Stewart, R. F.; Hall, S. R. *Org. Struct. Phys. Methods* **1971**, *3*, 73.
(33) The theoretical expression for the SOD contains a term for zero-point motion, which depends on the Debye temperatures of absorber and emitter.[34] As the Debye temperature is not the same for all materials, there is a contribution to the isomer shift, δ_{zpm}, which causes a dispersion of the points in the calibration plot for δ. However, since δ_{zpm} is estimated to be 0.01 mm s^{-1}, the scattering is within the standard deviation (0.04 mm s^{-1}) of our calibration curve, so that no corrections for δ_{zpm} are required.
(34) Hazony, Y. *Phys. Rev. B*: *Solid State* **1971**, *3* (3), 711.

Table 2. Results for Various Models for Power's Complex $[Fe(SR)_3]^-$ and Their Zn Analogues[a]

R	Zn−S (Å)	Fe−S (Å)	δ (mm s^{-1})	Q(Fe) (au)	Q(S) (au)	ΔE_Q [b]
H	2.362	2.361	0.507	1.040	−0.779	−1.882
CH_3	2.356	2.349	0.470	1.015	−0.544	−1.792
C_6H_5	2.365	2.350	0.484	1.015	−0.373	−1.792
$C_6H_3(C_2H_5)_2$ [c]	2.373	2.360	0.503	1.238	−0.296	−1.810
$C_6H_3(C(CH_3)_3)_2$ [c]	2.382	2.359	0.511	1.248	−0.376	−1.826
experiment	2.23 [d]	2.274 [e]	0.56 [e]			−0.83 [e]

[a] B3LYP/6-311G, point group symmetry C_{3h}, ground state: $^5A' = ...(z^2)^\beta$ (for Fe(II) compounds). Initial geometries for Fe compounds were the optimized geometries of Zn analogues. [b] Based on $Q = 0.16$ b. Accurate values for the EFGs can be computed only with accurate basis sets on Fe (e.g., Wachters (+f), 6-311+G*, and S (e.g., 6-311+G*) atoms in optimized structures. [c] Loose convergence criteria were set for geometry optimization (maximum force 2.5×10^{-3} au, rms force 1.67×10^{-3} au, maximum displacement 1.0×10^{-2} au, and rms displacement 6.67×10^{-3} au). [d] Reference 38. [e] References 4 and 5.

($\Delta\delta_{distance} > 0$), whereas the contributions have equal signs (Table 1) when bond lengths increase ($\Delta\delta_{distance} > 0$) as a result of electrochemical reduction ($\Delta\delta_{redox} > 0$). The data in Table 1 indicate that $\Delta\delta_{dist}$ dominates $\Delta\delta_{coord}$ in the cases listed. The same properties are found for a large number of complexes.[35] The dependence of δ on iron−ligand distance, R, is also listed in Table 1 (last column); $d\delta/dR$ decreases with increasing metal−ligand bond length, regardless of whether the bond length increases by adding ligands or electrons to the coordination site. The largest $d\delta/dR$ is found for the three-coordinate species in Table 1 (see also discussion of Power's complex). However, since the metal−ligand interactions in the three-coordinate species are stronger than those in the four-coordinate species, the reduction-induced distance change in the three-coordinate species is smaller than that in the four-coordinate one, to the extent that the corresponding increase in δ for the three-coordinate complex (0.32 mm s^{-1}) is about half that for the four-coordinate complex (0.58 mm s^{-1}). The present analysis underscores that any semiempirical theory for δ has to take the influence of the metal−ligand distance on this parameter into consideration (see sections 3.1.5 and 3.1.6).

We have also explored the intriguing possibility of correlating the isomer shifts with the redox potentials of iron compounds[36] but did not find any apparent general correlation.

3.1.3. Isomer Shift of Power's Trigonal Complex. The three-coordinate Fe−S compound, $[Fe(SR)_3]^-$ (R = C_6H_3-(t-Bu)$_2$), of Power and co-workers has served as a model for the trigonal iron sites in the earlier X-ray structure of FeMo cofactor[5] (see Introduction). Mössbauer studies support the approximate C_{3h} point group symmetry for this complex as derived from its X-ray structure and show that the ground state is $^5A'$, corresponding to a d_{z^2} β-HOMO.[4] The simplest computational model with R = H yields after geometry optimization an Fe−S bond length of 2.361 Å and $\delta = 0.507$ mm s^{-1} (Table 2). The difference between the calculated and observed shift (0.05 mm s^{-1}) is slightly outside the standard deviation of our calibration curve and may be attributed to an imperfect modeling of the ligand. Interestingly, however, the more realistic R = Me and R = Ar derivatives optimize at shorter distances, 2.349 and 2.350 Å, and the computed δ values of 0.470 and 0.484 mm s^{-1}, respectively, are in poorer agreement with the Mössbauer experiment. This result can be rationalized in terms of a decrease in the sulfur charges, which minimizes the inter-S Coulomb repulsions and allows the S atoms to approach the central metal ion. Again, contrary to what was expected, the Fe−S bond lengths further increase to 2.360 and 2.359 Å for R = $C_6H_3Et_2$ and C_6H_3(t-Bu)$_2$, respectively, in this instance due to repulsions between the positively charged members of the close Fe···H contacts, which appear to prevail over the diminished inter-S repulsions. Accordingly, the δ values increase to 0.503 and 0.511 mm s^{-1} and are again in reasonable agreement with experiment. A similar increase in δ has been shown to arise from the pseudocoordinative contacts in two-coordinate Fe−S complexes.[37] Comparable steric/charge effects are found in computational studies of three-coordinate Zn analogues[38] (Table 2).

3.1.4. Spin Ordering and Isomer Shifts. Calculations of ^{57}Fe isomer shifts for clusters with paramagnetic sites may have to cope with the possibility that this quantity is affected by spin ordering. In this section we argue that spin-ordering effects are small, provided one considers the average isomer shift, δ_{av}, taken over the iron sites in the cofactor cluster, so as to level out variations in δ due to heterogeneous electron distributions related to spin in the case of mixed valency. This view has the advantage that one can make a convenient choice for the spin state, which greatly facilitates the calculations and the identification of the orbital ground state among many possible states that can be envisaged in a cluster with the size of the cofactor. This approach is supported by the theory of exchange interactions between paramagnetic centers in solids formulated by Anderson in 1959.[39,40] Its basic premise is that these interactions can be treated in two separate steps. The first step deals with the ligand field, acting on the metal ions, and provides the states for the unpaired electrons at the selected ion, excluding the exchange interactions with the other magnetic ions. That these exchange effects do not disturb the local ligand-field wave function is experimentally supported by studies of superhyperfine interactions of ligand nuclei in dilute and concentrated versions of the same salt[41] as well as by studies of paramagnetic and antiferromagnetic temperature regions[42−45] (see also below). The second step concerns the problem of how the paramagnetic ions defined in the first step interact.

(35) Vrajmasu, V.; Münck, E.; Bominaar, E. L. Unpublished results.
(36) We have analyzed the correlation between δ_{calc} and ΔE_{SCF} for the redox couples of a number of iron complexes with various spin states, coordination numbers, and ligands (V.V., E.M., E.B., unpublished work).

(37) Evans, D. J.; Hughes, D. L.; Silver, J. *Inorg. Chem.* **1997**, *36*, 747.
(38) Gruff, E. S.; Koch, S. A. *J. Am. Chem. Soc.* **1989**, *111*, 8762.
(39) Anderson, P. W. *Phys. Rev.* **1959**, *115*, 2.
(40) Anderson, P. W. *Solid State Phys.* **1963**, *14*, 99.
(41) Clogston, A. M.; Gordon, J. P.; Jaccarino, V.; Peter, M.; Walker, L. R. *Phys. Rev.* **1960**, *117*, 1222.
(42) Shulman, R. G.; Jaccarino, V. *Phys. Rev.* **1956**, *103*, 1126.
(43) Shulman, R. G.; Wyluda, B. J.; Anderson, P. W. *Phys. Rev.* **1957**, *107*, 953.
(44) Shulman, R. G.; Jaccarino, V. *Phys. Rev.* **1957**, *108*, 1219.
(45) Jaccarino, V.; Shulman, R. G.; Stout, J. W. *Phys. Rev.* **1957**, *106*, 602.

The exchange interactions are much weaker than the ligand-field interactions considered in the first step and can therefore be treated with perturbation theory. Clearly, isomer shifts belong to the province of the first stage in Anderson's approach. The ferromagnetic state, in which the spins of the metal ions are aligned parallel, is an obvious choice for performing the first step. The state of maximum spin (S_{max}) is unique (in contrast to the states with lower spin) and can be expressed as a monodeterminantal wave function by choosing $M = S_{max}$. Because of Pauli antisymmetrization, the orbitals can be localized by performing a unitary transformation without changing the many electron states. This freedom has been used for defining the localized orbitals for storing the unpaired electrons in the exchange theory but is not required for calculating δ. The ferromagnetic state is ideally suited for performing molecular-orbital calculations and has therefore been adopted here. The premise that δ is insensitive to spin ordering is corroborated by the following observations: (a) The average isomer shift, 0.525 mm s^{-1}, for the serine-substituted two-iron ferredoxin in the valence-localized $S = {}^1/_2$ form ($Fd^1/_2$) is within the uncertainties the same as $\delta = 0.50$ mm s^{-1} for the valence-delocalized $S = {}^9/_2$ form ($Fd^9/_2$).[46] A similar consistency has been observed in the isomer shifts for the localized ($\delta(Fe^{3+}) = 0.59$ mm s^{-1} and $\delta(Fe^{2+}) = 0.94$ mm s^{-1} at 4.2 K, $\delta_{av} = 0.765$ mm s^{-1}) and delocalized ($\delta = 0.76$ mm s^{-1} at 4.2 K) conformational isomers of the mixed-valence diiron complex $(Mes_2ArCO_2)_3[Fe_2(OCHMe_2)_2]$.[47] (b) The consistency that exists in the dependence of site-averaged isomer shifts for bi-, tri-, and tetranuclear Fe−S clusters on formal oxidation state.[48] (c) The absence of an anomalous temperature dependence of the isomer shifts for clusters with exchange-coupled paramagnetic sites, as illustrated by the Mössbauer analysis of the valence-localized, $S = {}^9/_2$ complex $[Fe_2(salmp)_2]^{1-}$, where salmp = bis(salicylideneamino)-2-methylphenolate-(3−). The complex has exceptionally well-resolved magnetic 1.5-K spectra (see Figure 1 of ref 49) with distinguishable contributions for the Fe^{3+} and Fe^{2+} sites for which $\delta(Fe^{3+}) = 0.55$ mm s^{-1} and $\delta(Fe^{2+}) = 1.12$ mm s^{-1} ($\delta_{av} = 0.835$ mm s^{-1}) have been determined. At 225 K, the isomer shifts have declined to $\delta(Fe^{3+}) = 0.49$ mm s^{-1} and $\delta(Fe^{2+}) = 1.07$ mm s^{-1}.[50] The decline is exactly accounted for by the second-order Doppler shift, which was determined independently for the well-behaved diferrous complex. Moreover, at room temperature (Table 1 of Surerus et al.[49]) the complex exhibits a mixture of valence-localized and -delocalized (60%) forms. After correction for the second-order Doppler shift, both forms have δ values corresponding to $\delta(Fe^{3+})$, $\delta(Fe^{2+})$, and δ_{av} observed at 4.2 K. The exchange-coupling constant J of $[Fe_2(salmp)_2]^-$, obtained from magnetic susceptibility measurements, is -17.2 cm^{-1} ($H = JS_1S_2$), implying that ca. 56% of the molecules are in states with $S < {}^9/_2$ at 298 K. If the isomer shift of $[Fe_2(salmp)_2]^-$ were dependent on spin ordering, we would have observed an anomalous value of δ at high temperatures.

3.1.5. Influence of Inaccuracies in Optimized Metal−Ligand Distances on δ_{av}. The Fe−S distances obtained from spin-unrestricted B3LYP/6-311G geometry optimizations in both mononuclear sites and clusters are longer than the crystallographic distances. Moreover, the values for the discrepancies found for the clusters are systematically larger than those for the mononuclear sites. For example, the average Fe−S distance calculated for the rubredoxin model $[Fe^{3+}(SCH_3)_4]^-$ in the calibration set (2.356 Å) is longer than that obtained from the crystal structure (2.27 Å) by 0.086 Å; the values for the Fe^{2+} site are 2.479 Å for the geometry optimized structure and 2.36 Å for the X-ray structure.[51,52] Thus, the mononuclear Fe−S distances for B3LYP/6-311G are typically 0.1 Å longer than those deduced from X-ray data. The optimized Fe−S distance for the diferric cluster $[Fe_2S_2Cl_4]^{2-}$ is 2.346 Å and is 0.145 Å longer than the experimental value 2.201 Å;[53] the corresponding values for tetranuclear cluster $[Fe_4S_4Cl_4]^{2-}$ are 2.477 Å (calculated), 0.194 Å (deviation), and 2.283 Å (experiment). Addition of polarization and diffuse functions on all the atoms improves the computed metal−ligand bond lengths by about 0.04−0.05 Å. The combined inaccuracies, resulting from the computed Fe−S bond lengths and Fe−S−Fe angles, lead to sizable deviations between the computed and crystallographic intermetal separations (see below). Thus, the computed Fe···Fe separation is 3.305 Å for 6-311G and 3.075 Å for 6-311+G*. The dramatic improvement in separation between metals correlates with a decrease of the M−S−M angle from 89.6° (6-311G) to 83.8° (6-311+G*), approaching the average experimental angle 76.2°.[35] As demonstrated in section 3.1.2, the isomer shift is a sensitive function of metal−ligand distance. As a consequence, the increase in the optimized Fe−S distances for clusters with respect to those for the mononuclear complexes in the calibration set leads to systematically larger values for the isomer shifts. To correct for these spurious distance contributions to the isomer shift, we have used the chloride data in Table 1 as a reference for estimating the rate of change, $d\delta/dR \approx 0.5$ mm s^{-1}/Å. This value will be used in step 3 of the correction protocol discussed in section 3.1.6. The importance of this correction is illustrated by the calculations for δ in the delocalized-mixed-valence cluster $[Fe_4S_4Cl_4]^{2-}$. On the basis of our calibration curve, the average isomer shift, δ_{av}, for the B3LYP/6-311G optimized cluster is predicted to be 0.583 ± 0.04 mm s^{-1}. The difference (0.194 Å) between the calculated (2.283 Å) and observed (2.477 Å) Fe−S distances is greater, by 0.094 Å, than the Fe−S distance typically calculated for the calibration set. As a result, δ_{av} is

(46) Achim, C.; Bominaar, E. L.; Meyer, J.; Peterson, J.; Münck, E. *J. Am. Chem. Soc.* **1999**, *121*, 3704.
(47) Hagadorn, J. R.; Que, L., Jr.; Tolman, W. B.; Prisecaru, I.; Münck, E. *J. Am. Chem. Soc.* **1999**, *121*, 9760.
(48) Cen, W.; Lee, S. C.; Li, J.; MacDonnell, F. M.; Holm, R. H. *J. Am. Chem. Soc.* **1993**, *115*, 9515.
(49) Surerus, K. K.; Münck, E.; Snyder, B. S.; Holm, R. H. *J. Am. Chem. Soc.* **1989**, *111*, 5501.
(50) Achim, C.; Bominaar, E. L.; Staples, R. J.; Münck, E.; Holm, R. H. *Inorg. Chem.* **2001**, *40*, 4389.
(51) Dauter, Z.; Wilson, K. S.; Sieker, L. C.; Moulis, J.-M.; Meyer, J. *Proc. Natl. Acad. Sci. U. S. A.* **1996**, *93*, 8836.
(52) Min, T.; Ergenekan, C. E.; Eidsness, M. K.; Ichiye, T.; Kang, C. *Protein Sci.* **2001**, *10*, 613.
(53) Bobrik, M. A.; Hodgson, K. O.; Holm, R. H. *Inorg. Chem.* **1977**, *16*, 1851.

Table 3. Isomeric Shifts for Various Oxidation States of $[Fe_8XS_9Cl_2]^n$ (X = O, N, C) at the 6-311G-optimized Geometry (raw data)

		oxidation states					
model	n	no. of Fe^{2+}	no. of Fe^{3+}	S	δ (Fe_T) (mm s^{-1})	δ (Fe_{eq}) (mm s^{-1})	δ_{av} (mm s^{-1})
$[Fe_8CS_9Cl_2]$	0	0	8	20	0.414	0.303	0.331
	−2	2	6	19	0.421	0.369	0.382
	−4	4	4	18	0.560	0.405	0.444
$[Fe_8NS_9Cl_2]$	+1	0	8	20	0.425	0.302	0.333
	−1	2	6	19	0.414	0.374	0.384
	−3	4	4	18	0.536	0.423	0.451
	−5	6	2	17	0.533	0.548	0.544
$[Fe_8OS_9Cl_2]$	+2	0	8	20	0.432	0.298	0.331
	0	2	6	19	0.406	0.360	0.372
	−2	4	4	18	0.528	0.480	0.492
	−4	6	2	17	0.772	0.489	0.560

calculated too large by 0.5 mm s^{-1}/Å × 0.094 Å = 0.047 mm s^{-1}. The dδ/dR correction yields δ_{av} = 0.536 ± 0.04 mm s^{-1}, in excellent agreement with δ_{exp} = 0.52 mm s^{-1}.

3.1.6. Protocol for Predicting Average Isomer Shift of Cofactor. Next we focus on the average isomer shift, δ_{av}, taken over the Fe sites of FeMoco. Data for δ_{av} are available for FeMoco in *Azotobacter vinelandii*[2] (*Av*, 0.41(2) mm s^{-1} at 4.2 K) and *Clostridium pasteurianum*[54] (*Cp*, 0.40(2) mm s^{-1} at 4.2 K), for the cofactor extracted from *Av*[55−57] (0.38 mm s^{-1} at 90 K), for the iron−vanadium cofactor (FeVco) from *Azotobacter vinelandii*[58] (*Av*, 0.39(2) mm s^{-1} at 80 K), and the iron-only cofactor (FeFeco) from *Rhodobacter capsulatus*[59] (*Rc*, 0.40(2) mm s^{-1} at 77 K). To compare these values with the predictions of the semiempirical theory developed above, the calculated values for the terminal (δ_T) and equatorial (δ_{Eq}) sites of the $[Fe_8S_9Cl_2]^n$ cofactor model (Table 3) were subjected to a conversion algorithm, consisting of four steps.

Step 1 accounts for the effect on δ_{av} of replacing the six-coordinate molybdenum in FeMoco by one of the Fe_TS_3Cl sites in the structure of the computational model. We consider Fe^{3+} to be the most appropriate oxidation state for the terminal iron that replaces the molybdenum site in the FeMoco, primarily because the charge of the terminal $Fe^{3+}Cl^-$ moiety of the model cluster is equal to that of dicarboxylate-coordinate Mo^{4+} in M^N (see Introduction) and because the corresponding site is not Fe^{2+} in FeFeco. Therefore, we have redistributed any electronic charge accumulated upon reduction of the "$[0Fe^{2+}7Fe^{3+}]$" model complex $[(Fe^{3+})_8S_9Cl_2]^{4+}$ at one of the Fe_TS_3Cl sites over the remaining seven irons of the model before this site can be represented by Mo^{4+}; in the following $[nFe^{2+}(n-7)Fe^{3+}]$ represents the seven core sites of FeMoco. The DFT-based isomer shifts exhibit a nearly linear dependence on the formal oxidation state. This property is illustrated by the results of calculations for the Fe−S model cubane $[Fe_4S_4Cl_4]^{n-}$ shown in SI Figure S.2. The slope of the linear relationship, 0.37 mm s^{-1}/e^-, has been used to convert the reduction-induced changes in δ_T (Table 3) into fractional electron numbers. For example, the increment $\Delta\delta_T$ = 0.533 − 0.425 mm s^{-1} = 0.108 mm s^{-1} (Table 3) obtained in passing from the all-Fe^{3+} form to the $[4Fe^{2+}3Fe^{3+}]$ cluster yields $\Delta\delta_T$/0.37 = 0.29 redistributable electrons. The increase in δ_{av} occurring upon redistribution of this charge over the seven remaining sites of the cofactor model has been evaluated by interpolating between the averaged isomer shifts for the $[6Fe^{2+}1Fe^{3+}]$ and $[4Fe^{2+}3Fe^{3+}]$ clusters, i.e., $\Delta\delta_{av}$ = $^1/_2$ $[\delta_{av}(6Fe^{2+}1Fe^{3+}) - \delta_{av}(4Fe^{2+}3Fe^{3+})]$ × 0.29 mm s^{-1} = +0.013 mm s^{-1}. The occupation numbers of the terminal sites obtained from our calculations are probably slightly larger than those for the cysteine-bound site in the cofactor because of electron delocalization arising from the ferromagnetic spin ordering adopted here. On the other hand, the delocalization is counteracted by the heteroleptic coordinations of the terminal irons, which differentiates these sites from the equatorial ones and makes them less accessible to the itinerant electrons in the cluster. As can be seen from the example given, the corrections of step 1 are small and do not affect the assessment of the oxidation state of M^N. Since a balanced basis set for Mo of 6-311G quality was lacking, the correction procedure was examined by replacing one of the terminal atoms by Ga^{3+}, i.e., for $[Fe_7GaNS_9Cl_2]^{n-}$. While the conclusion regarding the formal oxidation state of M^N remained unchanged (section 3.1.7), the computational time increased by a factor of 4 due to symmetry lowering from D_{3h} to C_{3v}.

Step 2 corrects for the changes in δ_T arising from the replacement of the terminal cysteinyl sulfur by a chloride. This correction ($\Delta\delta_T \approx -0.08$ mm s^{-1}; the minus sign indicates that the calculated value is an overestimate) is estimated from the isomer shifts for the cubane $[(Fe^{2.5+})_4S_4Cl_4]^{2-}$ (δ_{exp} = 0.52 mm s^{-1}) and the $[(Fe^{2.5+})_4S_4(S_{cys})_4]^{2-}$ cluster in ferredoxins (δ_{exp} = 0.42−0.45 mm s^{-1}) and applied indiscriminately to both the oxidized and (partially) reduced states of the terminal iron. The correction of step 2 decreases δ_{av} by ~0.01 mm s^{-1}.

Step 3 corrects for spurious contributions to δ_{Eq} and δ_T that arise from atypical discrepancies between the calculated and crystallographic iron−sulfur distances, taking the calibration set as a reference (see above). The mononuclear Fe−S distances for B3LYP/6-311G are typically 0.1 Å longer than those deduced from X-ray data. A comparison of the latter discrepancy with the ones found between the optimized cluster $[4Fe^{2+}3Fe^{3+}$:N] and the crystallographic data (Table 4) reveals atypical deviations: $\Delta(Fe_{Eq} - S_{Eq})$ = (2.295 − 2.226) Å = 0.069 Å, $\Delta(Fe_{Eq} - S_T)$ = (2.432 − 2.270) Å =

(54) Huynh, B. H.; Henzl, M. T.; Christner, J. A.; Zimmermann, R.; Orme-Johnson, W. H.; Münck, E. *Biochim. Biophys. Acta* **1980**, *623*, 124.
(55) Rawlings, J.; Shah, V. K.; Chisnell, J. R.; Brill, W. J.; Zimmermann, R.; Münck, E.; Orme-Johnson, W. H. *J. Biol. Chem.* **1978**, *253*, 1001.
(56) The SOD-corrected value, δ_{av} = 0.39(2) mm s^{-1}, is the same as that in the *Av* protein from which the cofactor was isolated. This result suggests that the influence of protein environment on δ_{av}, notably, of hydrogen bonding to protein residues identified by ^{1}H ENDOR in *Av*, is minor.[57] To examine the effect of the medium, we have performed a number of calculations of complexes placed in different dielectrics and found that the isomer shift does not noticeably change if the dielectric constant is changed from its value in vacuum (ϵ = 1) to a value more suitable for a protein medium (ϵ = 4).
(57) Lee, H.-I.; Cameron, L. M.; Hales, B. J.; Hoffman, B. M. *J. Am. Chem. Soc.* **1997**, *119*, 10121.
(58) Ravi, N.; Moore, V.; Lloyd, S. G.; Hales, B. J.; Huynh, B. H. *J. Biol. Chem.* **1994**, *269*, 20920.
(59) Krahn, E.; Weiss, B. J. R.; Kröckel, M.; Groppe, J.; Henkel, G.; Cramer, S. P.; Trautwein, A. X.; Schneider, K.; Müller, A. *J. Biol. Inorg. Chem.* **2002**, *7*, 37.

Table 4. Computed Structure Data

system [nFe^{2+}:X]	cluster charge	angles (deg) Fe_{Eq} S_{Eq} Fe_{Eq}	angles (deg) Fe_T S_T Fe_{Eq}	angles (deg) Fe_{Eq} S_T Fe_{Eq}'	distances (Å) $Fe_{Eq}X$	$S_{Eq}X$	$Fe_{Eq}Fe_{Eq}$	$Fe_{Eq}Fe_T$	$Fe_{Eq}S_{Eq}$	$Fe_{Eq}S_T$	Fe_TS_T	Fe_TCl
[0Fe^{2+}8Fe^{3+}:C]	0	79.5	89.3	80.5	2.295	3.519	2.878	3.400	2.251	2.395	2.442	2.179
[2Fe^{2+}6Fe^{3+}:C]	−2	71.3	88.1	76.4	2.196	3.602	2.661	3.373	2.283	2.447	2.402	2.260
[4Fe^{2+}4Fe^{3+}:C]	−4	65.0	86.5	75.2	2.161	3.729	2.512	3.375	2.337	2.496	2.432	2.421
[0Fe^{2+}8Fe^{3+}:N]	+1	81.4	90.0	83.5	2.326	3.505	2.910	3.418	2.231	2.361	2.474	2.150
[2Fe^{2+}6Fe^{3+}:N]	−1	70.5	88.2	80.4	2.214	3.632	2.676	3.358	2.257	2.403	2.424	2.213
[4Fe^{2+}4Fe^{3+}:N]	−3	65.9	86.7	78.5	2.170	3.702	2.495	3.351	2.295	2.432	2.450	2.334
[6Fe^{2+}2Fe^{3+}:N]	−5	62.1	86.9	74.9	2.157	3.797	2.421	3.398	2.348	2.543	2.393	2.502
[0Fe^{2+}8Fe^{3+}:O]	+2	88.9	91.0	90.7	2.475	3.510	3.109	3.460	2.220	2.343	2.504	2.130
[2Fe^{2+}6Fe^{3+}:O]	0	73.2	88.5	87.7	2.320	3.694	2.677	3.279	2.239	2.371	2.443	2.178
[4Fe^{2+}4Fe^{3+}:O]	−2	79.2	88.1	86.5	2.381	3.639	2.891	3.350	2.268	2.390	2.427	2.265
[6Fe^{2+}2Fe^{3+}:O]	−4	69.6	86.2	82.1	2.259	3.735	2.642	3.387	2.316	2.417	2.539	2.454
FeMoco	?	71.4	71.8	71.6	1.999	3.326	2.589	2.667	2.226	2.270	2.278	

Table 5. Site-Averaged Isomer Shifts, δ_{av} (mm s^{-1})

system	C	N	O	
[0Fe^{2+}7Fe^{3+}:X]	0.307	0.325	0.322	
[2Fe^{2+}5Fe^{3+}:X]	0.347	0.367	0.355	
[4Fe^{2+}3Fe^{3+}:X]	**0.386**	**0.424**	0.484	
[6Fe^{2+}1Fe^{3+}:X]		0.494	0.528	
FeMoco				0.41(2)
FeVco				0.40(2)
FeFeco				0.40(2)

0.162 Å, and $\Delta(Fe_T - S_T) = (2.450 - 2.278)$ Å $= 0.172$ Å. Taking the deviation ~0.1 Å of mononuclear complexes as a reference, the additional (cluster-related) errors in the averages of the computed distances are then $(-0.031 + 2 \times 0.062)/3 = 0.031$ Å for $Fe_{Eq}-S_T$ and $3 \times 0.072/4$ Å $= 0.054$ Å for Fe_T-S_T. As shown in section 3.1.2, longer metal−ligand distances give rise to larger isomer shifts. By use of the slope $d\delta/dR = 0.5$ mm s^{-1}/Å for three- and four-coordinate sites, the values of δ_{Eq} and δ_T calculated with our semiempirical theory for the isomer shift are too high by $-\Delta\delta_{Eq} \approx 0.031 \times 0.5$ mm s^{-1} ≈ 0.015 mm s^{-1} and $-\Delta\delta_T \approx 0.054 \times 0.5$ mm s^{-1} $= 0.027$ mm s^{-1}, respectively.

Step 4 applies the corrections defined in the previous steps to the semiempirical (se) results for δ_{Eq} and δ_T (Table 3), $\delta = \delta_{se} + \sum_{i=1}^{3} \Delta\delta_i$, and averages the corrected values, $\delta_{av} = {}^1/_7(\delta_T + 6\delta_{Eq})$. For example, the values for [4Fe^{2+}-3Fe^{3+}:N] are $\delta_T = (0.536 + 0.013 - 0.080 - 0.027)$ mm s^{-1} $= 0.442$ mm s^{-1} and $\delta_{Eq} = (0.423 - 0.015 + 0.013)$ mm s^{-1} $= 0.421$ mm s^{-1} and yield $\delta_{av} = {}^1/_7(0.442 + 6 \times 0.421)$ mm s^{-1} $= 0.424$ mm s^{-1} (Table 5). Note that the corrections of steps 1 and 3 affect the final δ_{av} by only 0.004 mm s^{-1}.

3.1.7. Oxidation State of M^N. Table 5 lists the calculated δ_{av} values for various assumed oxidation states of the M cluster for X = C, N, and O. The best agreement with the experimental data for the state M^N is obtained in the calculations for the clusters [4Fe^{2+}3Fe^{3+}:C] and [4Fe^{2+}3Fe^{3+}:N]. Note that the calculated δ_{av} values for [Mo^{4+}6Fe^{2+}1Fe^{3+}] are distinctly higher. Thus, the present analysis suggests [Mo^{4+}4Fe^{2+}3Fe^{3+}] as the most likely formulation of M^N, in agreement with the assignment proposed by Yoo et al.[2] but in disagreement with the [Mo^{4+}6Fe^{2+}1Fe^{3+}] formulation, independently suggested by Hoffman et al.[3] and Noodleman et al.[6] The one-electron oxidized state of FeMoco, the $S = 0$ state M^{OX}, has $\delta_{exp} = 0.36$ mm s^{-1}. This value together with $\delta_{av} = 0.41$ mm s^{-1} for M^N suggests that $d\delta_{av}/dn \approx 0.05$ mm s^{-1}/e$^-$. The slope can be compared with half the difference of the δ_{av} values calculated for the [2Fe^{2+}5Fe^{3+}:X] and [4Fe^{2+}3Fe^{3+}:X] oxidation states, that is, 0.03 mm s^{-1} for X = N, 0.02 mm s^{-1} for C, and 0.06 mm s^{-1} for O. The observed and calculated numbers for $d\delta_{av}/dn$ are quite similar, although there is a slightly better agreement for N. The accumulated change, i.e., $7 \times 0.04 = 0.28$ mm s^{-1} per electron, corresponds to the increase in the isomer shift of a representative site in the cofactor upon reduction by one full electron. This change is small but typical for three-coordinate iron (see section 3.1.2). Thus, inasmuch as the isomer shift is concerned, the central atom X seems to act as a weak ionic ligand to the equatorial irons in the cofactor (for comparison, the corresponding change for four-coordinate sites is typically 0.45 mm s^{-1} rather than 0.28 mm s^{-1}). Given that $d\delta_{av}/dn \approx 0.04$ mm s^{-1}/e$^-$, the error margin of the calculated values for δ_{av} should be within 0.04 mm s^{-1} in order to predict the oxidation state within an accuracy of ±1 electron. This condition is fulfilled by the standard deviation of our calibration set (i.e., 0.04 mm s^{-1}) and admits [4Fe^{2+}3Fe^{3+}:C], [2Fe^{2+}5Fe^{3+}:N], and [4Fe^{2+}3Fe^{3+}:N] as possible assignments for M^N (Table 5), among which the two [4Fe^{2+}3Fe^{3+}] states for C and N give the best agreement (see above). This result is supported by the redox potential calculations of Dance.[60] The negative overall charge of the preferred oxidation state [Mo^{4+}4Fe^{2+}3Fe^{3+}9S^{2-}X^{n-}:homocitrate^{3-}]$^{n-}$ (n = 2, 3, 4) is consistent with the negative charge of the extracted cofactor inferred from DEAE-binding studies,[61,62] counterion chromatography,[63] and electrophoretic measurements.[64]

3.1.8. The Influence of the Interstitial Atom X on the Isomer Shift of Cofactor. The effect of X on the average isomer shift has been investigated for X = C, N, and O (Table 6), adopting a symmetrized cofactor model with geometrical parameters as in the X-ray structure of the M

(60) Dance, I. *Chem. Commun.* (*Cambridge, U.K.*) **2003**, 324.
(61) McLean, P. A.; Wink, D. A.; Chapman, S. K.; Hickman, A. B.; McKillop, D. M.; Orme-Johnson, W. H. *Biochemistry* **1989**, *28*, 9402.
(62) Wink, D. A.; McLean, P. A.; Hickman, A. B.; Orme-Johnson, W. H. *Biochemistry* **1989**, *28*, 9407.
(63) Huang, H. Q.; Kofford, M.; Simpson, F. B.; Watt, G. D. *J. Inorg. Biochem.* **1993**, *52*, 59.
(64) Yang, S. S.; Pan, W. H.; Friesen, G. D.; Burgess, B. K.; Corbin, J. L.; Stiefel, E. I.; Newton, W. E. *J. Biol. Chem.* **1982**, *257*, 8042.

Table 6. Isomeric Shifts for Various Oxidation States of $[Fe_8XS_9Cl_2]^n$ (X = O, N, Ø) at the X-ray Averaged Geometry

		oxidation states					
model	n	no. of Fe^{2+}	no. of Fe^{3+}	S	$\delta(Fe_T)$ (mm s^{-1})	$\delta(Fe_{Eq})$ (mm s^{-1})	δ_{av} (mm s^{-1})
$[Fe_8OS_9Cl_2]$	0	2	6	19	0.325	0.266	0.280
	−2	4	4	18	0.346	0.363	0.359
	−4	6	2	17	0.532	0.420	0.448
$[Fe_8NS_9Cl_2]$	−1	2	6	19	0.324	0.256	0.273
	−3	4	4	18	0.360	0.342	0.347
	−5	6	2	17	0.553	0.392	0.433
$[Fe_8S_9Cl_2]$	+2	2	6	19	0.325	0.102	0.158
	0	4	4	18	0.292	0.166	0.198
	−2	6	2	17	0.336	0.244	0.267

Table 7. Mulliken Charges

	Mulliken charges					
state	X	Fe_{Eq}	Fe_T	S_{Eq}	S	Cl
$[0Fe^{2+}8Fe^{3+}:C]$	−2.35	1.28	1.29	−0.64	−0.87	−0.41
$[2Fe^{2+}6Fe^{3+}:C]$	−2.47	1.27	1.26	−0.85	−0.98	−0.60
$[4Fe^{2+}4Fe^{3+}:C]$	−2.44	1.23	1.24	−1.04	−1.14	−0.76
$[0Fe^{2+}8Fe^{3+}:N]$	−1.71	1.30	1.22	−0.54	−0.83	−0.30
$[2Fe^{2+}6Fe^{3+}:N]$	−1.83	1.18	1.29	−0.72	−0.94	−0.51
$[4Fe^{2+}4Fe^{3+}:N]$	−1.84	1.26	1.16	−0.91	−1.09	−0.71
$[6Fe^{2+}2Fe^{3+}:N]$	−1.81	1.24	1.11	−1.17	−1.20	−0.84
$[0Fe^{2+}8Fe^{3+}:O]$	−1.20	1.31	1.22	−0.49	−0.81	−0.19
$[2Fe^{2+}6Fe^{3+}:O]$	−1.30	1.14	1.29	−0.61	−0.92	−0.41
$[4Fe^{2+}4Fe^{3+}:O]$	−1.18	1.26	1.20	−0.98	−1.07	−0.59
$[6Fe^{2+}2Fe^{3+}:O]$	−1.32	1.25	1.13	−1.05	−1.20	−0.83

cluster, regardless of the choice for X and oxidation state. X has the effect to raise the value for δ_{av} by 0.15 ± 0.03 mm s^{-1} through charge donation to the irons. An increase in isomer shift is a common manifestation of the reduction of iron sites in iron−sulfur and other centers. Since the capacity of the Fe and S sites in $[nFe^{2+}(7-n)Fe^{3+}:X]$ to accept electrons diminishes as the cluster becomes further reduced, one would expect that the difference in the isomer shifts for $[nFe^{2+}(7-n)Fe^{3+}:X]$ and the donor-site-lacking cluster $[nFe^{2+}(7-n)Fe^{3+}:Ø]$ decreases with the number of cluster electrons. However, the data listed in Table 6 show the opposite behavior. For example, one finds the increments in δ_{av} of 0.112 mm s^{-1} for $n = 6$, 0.149 mm s^{-1} for $n = 4$, and 0.166 mm s^{-1} for $n = 2$, due to the presence of the central nitride. The increase depends on two factors: First, as discussed in section 3.1.2, the increment in δ per added electron increases with the number of neighbors placed at a constant distance from the iron center. Second, the population data in Table 7 show that the electron donation from the central atom is almost independent of the oxidation state, such that the first factor prevails. The isomer shifts listed in Table 6 are systematically lower than the isomer shifts for the corresponding cofactor states, because the structures were not relaxed after adding electrons. If we make the plausible assumption that the iron centers in the resting forms of FeFeco and FeMoco are in similar oxidation states, then we are forced to conclude that the iron-only cluster, for which no crystal structure is available, contains a central atom, because δ_{av} of FeFeco without central atom would be smaller by 0.1−0.2 mm s^{-1} than the value for FeMoco, at variance with experiment. Furthermore, the present analysis supports the presence of a central atom in the oxidation states M^{OX} and M^R because the isomer shifts of these states would be much lower than those observed in the absence of X. This conclusion suggests X to be a structural element of the cofactor that is retained during the redox activity of the cluster.

3.1.9. The Nature of the Central Atom. The δ_{av} values listed in Table 5 for X = O are either significantly smaller or larger than those observed. We have presently no explanation for the large change in δ_{av} in the reduction step from $[2Fe^{2+}5Fe^{3+}:O]$ to $[4Fe^{2+}3Fe^{3+}:O]$ and cannot exclude a methodological artifact as its cause. The possibility of a central oxygen atom was ruled out[60,65] on the basis of the unreasonable values obtained for the nonbonding $Fe_{Eq}-Fe_{Eq}$ distances from DFT calculations (see Figure 1 for definition of distances). In accordance with the earlier results, the present calculations predict that the $Fe_{Eq}-Fe_{Eq}$ distances increase in the order C < N < O (Table 4). This property holds for each oxidation state, $[nFe^{2+}(7-n)Fe^{3+}:X]$, with the exception of $[4Fe^{2+}3Fe^{3+}:C]$ and $[4Fe^{2+}3Fe^{3+}:N]$, which have nearly identical separations between the equatorial irons. However, the Fe−Fe separations should be considered with caution when used for identifying the central atom, X. Without having prior knowledge of the oxidation state, $Fe_{Eq}-Fe_T$ distances that match the experimental value within 0.1 Å can be found for any choice of the central atom (Table 4). Moreover, the $Fe_{Eq}-Fe_T$ distances are systematically larger than those observed, which corroborates the notion that we can at best predict the trends but not the precise values of the nonbonding distances at the current level of theory. Fortunately, unlike the metal−ligand distances, the separations between the Fe sites have little influence on the average isomer shift, δ_{av}, and it is therefore unlikely that inaccuracies in these quantities could impair the assignment of the oxidation state of M^N. The $Fe_{Eq}-S_{Eq}$ distances are in good agreement with experiment. Although the agreement is best in the (experimentally inaccessible) higher oxidation states $[0Fe^{2+}7Fe^{3+}:X]$ and $[2Fe^{2+}5Fe^{3+}:X]$, we consider our results to be supportive of the lower oxidation levels, because the $Fe_{Eq}-S_{Eq}$ distances therein are longer than those observed by ∼0.1 Å, as anticipated from the optimizations for the calibration set. A scrutiny of Table 4 reveals that all metal−ligand distances, $Fe_{Eq}-S_{Eq}$, $Fe_{Eq}-S_T$, Fe_T-S_T, and Fe_T-Cl, increase in the order O < N < C in each oxidation state $[nFe^{2+}(7-n)Fe^{3+}:X]$ and the distances $Fe_{Eq}-S_{Eq}$ and Fe_T-Cl increase upon reduction of the cluster. The two trends have a common cause, namely, an increase in the number of electrons stored in the cluster that is brought about by either reduction or enhanced electron donation from the central atom in the series $O^{2-} < N^{3-} < C^{4-}$. The distances $Fe_{Eq}-S_T$ = 2.36−2.50 Å and Fe_T-S_{Eq} = 2.39−2.54 Å, though partly following the same trend, behave more erratically and appear to reflect certain details of the electronic structure for which they were obtained.

3.1.10. Quadrupole Splittings of Trigonal Sites. Among the puzzling features of the M centers have been the small ΔE_Q values of the equatorial Fe sites.[2] To get some insight

(65) Hinnemann, B.; Nørskov, J. K. *J. Am. Chem. Soc.* **2003**, *125*, 1466.

Table 8. Distance Dependence of Quadrupole Splitting, ΔE_Q[a]

B3LYP/6-311G					B3LYP/6-311++G**				
$Fe^{2+}(z^2)$	$[Fe^{3+}(SH)_3]^0$		$[Fe^{2+}(SH)_3]^{1-}$		$Fe^{2+}(z^2)$	$[Fe^{3+}(SH)_3]^0$		$[Fe^{2+}(SH)_3]^{1-}$	
ΔE_Q (mm s^{-1})	Fe−S (Å)	ΔE_Q (mm s^{-1})	Fe−S (Å)	ΔE_Q (mm s^{-1})	ΔE_Q (mm s^{-1})	Fe−S (Å)	ΔE_Q (mm s^{-1})	Fe−S (Å)	ΔE_Q (mm s^{-1})
	2.256[b]	2.372	2.361[b]	−1.882[c]		2.256[b]	2.257	2.337[b]	−1.540
	2.246	2.423	2.351	−1.844		2.246	2.300	2.327	−1.506
−4.65[c]	2.236	2.473	2.341	−1.807	−4.51	2.236	2.343	2.317	−1.472
	2.226	2.523	2.331	−1.768		2.226	2.386	2.307	−1.437
	2.216	2.574	2.321	−1.729		2.216	2.428	2.297	−1.401
	2.206	2.624	2.311	−1.689		2.206	2.471	2.287	−1.364
ΔE_Q	−5.036(FeS) + 13.731		−3.850(FeS) + 7.208		ΔE_Q	−4.268(FeS) + 11.885		−3.520(FeS) + 6.697	

[a] $Q = 0.16$ b and conversion factor $^1/_2\ eQ = -1.617$ mm s^{-1}/au. [b] Distance from geometry optimization of model. [c] The signs of ΔE_Q are the reversed signs of the principal component of the EFG with the largest magnitude. The axis of this component is normal to the molecular plane in all cases considered here.

into this property, we have performed B3LYP calculations in the high-spin states of the ferric and ferrous forms of the trigonal planar (computational) model complex $[Fe(SH)_3]$. The results of the calculations for two standard basis sets are listed in Table 8. The first column, for each basis set, gives ΔE_Q for the substate of the degenerate $L = 2$ manifold of a free d^6 iron ion in which a d_{z^2} orbital is doubly occupied. This orbital represents the ground state of a 3d electron in a trigonal crystal field. ΔE_Q for d_{z^2} is negative and provides an estimate of the valence contribution, ΔE_Q(val), in trigonal planar complexes.[4,66] The negative ΔE_Q values listed for the d^6 complex $[Fe^{3+}(SH)_3]^-$ (5th and 10th columns) arise from a dominant d_{z^2} valence contribution to the EFG. The first entry of the second, fourth, seventh, and ninth column is the Fe−S distance obtained from C_{3h}-contrained geometry optimizations for the basis set and oxidation state indicated; the subsequent lines in these columns differ from the preceding ones by an increment of −0.01 Å and the ΔE_Q values calculated for these distances are tabulated in the respective rows. The results listed for $[Fe^{3+}(SH)_3]^0$ concern the spherically symmetric d^5 configuration of a high-spin ferric ion for which ΔE_Q vanishes in the ligand-free form. However, the calculations show that ΔE_Q of the ferric complexes has a large positive value (∼+2.5 mm s^{-1}) from which we conclude that the ligand contributions, ΔE_Q(lig), are sizable. Large ligand contributions to ΔE_Q are characteristic of linear, trigonal, or square-planar coordinations and are absent in strictly octahedral or tetrahedral sites for which ΔE_Q(lig) vanishes for reasons of symmetry. The positive sign of ΔE_Q(lig) in $[Fe^{3+}(SH)_3]^0$ reflects the oblate distribution of the negative charges arising from the planar arrangement of the Fe−S bonds. It is common to label the principal axes of the traceless EFG tensor according to the eigenvalues $|V_{xx}| \le |V_{yy}| \le |V_{zz}|$. The x and y axes of the EFG tensors for both the valence and summed ligand contributions to the EFG in $[Fe^{3+}(SH)_3]^-$ are in the molecular plane. Each sulfur ligand contributes an EFG of which the component with largest magnitude is aligned along the corresponding Fe−S bond. As each bond represents a prolate distribution of negative charge, the sign of the EFG component along that bond is negative. Accordingly, the EFG components along the normal of the molecular plane for the individual iron−sulfur bonds are positive and add up to give a positive total ligand contribution. The EFG component from, and along, a single Fe−S bond in $[Fe^{3+}(SH)_3]^0$ is estimated to be as much as $-^2/_3\Delta E_Q(\text{lig}) \approx -1.7$ mm s^{-1}. The valence and ligand contributions to the EFG along the z axis of $[Fe^{3+}(SH)_3]^-$ have opposite signs, leading to a significant cancellation and to net quadrupole splittings whose magnitudes are smaller than that of the free d_{z^2} ion.

Table 8 reveals that ΔE_Q is a decreasing function of the Fe−S distances. The ΔE_Q values decay linearly with distance, as indicated in the bottom row of Table 8. Using the linear relationships obtained for basis set 6-311G, we estimated the values $\Delta E_Q(\text{lig}) = +2.50$ mm s^{-1} and $\Delta E_Q(2+) = -1.38$ mm s^{-1} for $[Fe^{2+}(SH)_3]^-$ at the experimental equilibrium distance $(Fe-S)_{exp} = 2.23$ Å of Power's trigonal planar complex.[5] To verify the validity of the relation $\Delta E_Q(2+) \approx \Delta E_Q(\text{val}) + \Delta E_Q(\text{lig})$, we have compared $\Delta E_Q(\text{val}) = -1.38$ mm s^{-1} − 2.50 mm s^{-1} = −3.88 mm s^{-1} for $[Fe^{2+}(SH)_3]^-$ with the free ion value for this quantity, −4.65 mm s^{-1}; the corresponding values for basis 6-311++G** are −3.52 and −4.51 mm s^{-1}. The molecular value for ΔE_Q(val) is smaller in magnitude than the free ion value by 0.77 and 0.99 mms^{-1} for the two respective bases. A detailed analysis of the minority-spin d_{z^2} orbital state reveals that the reduction results from the symmetry allowed admixture of the iron 4s (A_1) orbital into d_{z^2} (A_1) in the trigonal ligand field of the model complex. Partial cancellation of the admixture-diminished valence terms of the ferrous-like equatorial irons against the ligand terms, arising from the trigonal-type sulfur coordinations of these sites, explains the ΔE_Q values of the cofactor (ranging from −0.7 to −1 mm s^{-1} in M^N; $|\Delta E_Q|$ of high-spin ferrous sites are typically greater than 2.5 mm s^{-1}) and of the equatorial irons in a recent synthetic P-cluster model, containing a hexa-iron coordinate sulfide but terminal and bridging amines.[67] The value $\Delta E_Q(2+) = -1.38$ mm s^{-1} calculated with the 6-311G basis is somewhat larger in magnitude than that observed for Power's complex $\Delta E_Q(\text{exp}) = -0.83$ mm s^{-1}. Agreement with the experiment, however, improves noticeably ($\Delta E_Q(2+) = -1.15$ mm s^{-1}) by extending the basis with diffuse and polarization functions. The calculated ΔE_Q values are not yet as satisfactory as the δ_{av} values because an extensive cancellation of

(66) Andres, H.; Bominaar, E. L.; Smith, J. M.; Eckert, N. A.; Holland, P. L.; Münck, E. *J. Am. Chem. Soc.* **2002**, *124*, 3012.

(67) Ohki, Y.; Sunada, Y.; Honda, M.; Katada, M.; Tatsumi, K. *J. Am. Chem. Soc.* **2003**, *125*, 4052.

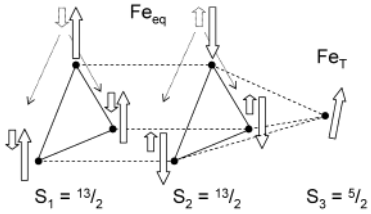

Figure 2. Proposed scheme for valence delocalization and spin ordering in state M^N of FeMoco. Black dots represent iron sites. Large block arrows are Fe(d^5) spins, $S_{local} = 5/2$. Small block arrows indicate $S = 1/2$ minority spins of electrons (solid) and holes (hashed) in Fe(d^6). Dotted arrows symbolize hole delocalization.

oppositely signed terms inevitably results in small values with large relative errors. In summary, the fact that the quadrupole splittings in the cofactor can be described by models with trigonal sites confirms the conclusion drawn from the analysis of the isomer shifts that the individual bonds between the equatorial irons and the central atom X are weak. Notwithstanding their individual weakness, the collective stabilization energy of six coordination bonds may turn the central atom into a rigid element of the cofactor structure.

3.1.11. Is an [4Fe^{2+}3Fe^{3+}] Formulation of M^N Consistent with the *A* Values? The Mössbauer studies of Yoo et al.[2] and ENDOR studies of Hoffman and co-workers[3] have provided a complete set of ^{57}Fe magnetic hyperfine tensors for the seven Fe sites in the cofactor state M^N. The isotropic parts of these tensors, A_{iso}, have large negative values for three iron sites (-17.1, -18.0, -11.8 MHz; average $\langle A_1\rangle_{av} \approx -16$ MHz) are positive for another three irons ($+11.7$, $+11.7$, $+9.3$ MHz; average $\langle A_2\rangle_{av} \approx +11$ MHz). A seventh site has a small, negative A value, $A_3 \approx -4$ MHz; this site was labeled A^4 by Yoo et al.[2] Lovell et al.[6,23] have interpreted these values using spin-coupling schemes pertaining to the [6Fe^{2+}1Fe^{3+}] formulation of M^N. Their most accurate descriptions involve schemes in which A_3 is assigned to one of the equatorial Fe sites. In the following we offer considerations that show that the oxidation state [4Fe^{2+}3Fe^{3+}] proposed for M^N is compatible with the experimental data. Figure 2 depicts the spin ordering and valence delocalization (dotted arrows) for an $S = 3/2$ state that yield the salient features of the magnetic hyperfine interactions in M^N. The seven Fe sites of the cofactor have been grouped into two triangles, each one comprising the three equatorial irons of a cuboidal moiety, and a terminal site (the spin of the Mo^{IV} site is zero). The triangles have the formal oxidation states [2Fe^{2+}Fe^{3+}] and are considered valence-delocalized, [3Fe$^{2.33+}$], with parallel spin orderings; thus, $S_1 = S_2 = 13/2$. The terminal site is Fe^{3+} and has spin $S_3 = 5/2$. S_3 is first coupled to S_2 to yield the intermediate spin S_{23} for the 4Fe moiety of the cofactor; S_{23} is subsequently antiparallel coupled to S_1 of the Mo3Fe moiety: $|(S_1(S_2,S_3)S_{23})S\rangle = |(13/2(13/2,5/2)5)3/2)\rangle$. The spins S_2 and S_3 are not completely antiparallel in the composite spin $S_{23} = 5$, as they would be for $S_{23} = 4$, but are slightly "canted". The effective A values, which refer to the total spin $S = 3/2$, can be expressed in the present model as $\langle A_1\rangle_{av} = +a_{int}$, $\langle A_2\rangle_{av} = -7/9 a_{int}$, and $A_3 = +1/3 a_{int}$ in terms of the intrinsic A value of a single site, a_{int}, which is assumed to have the same value for all six equatorial Fe sites. Given the predominant quasi-trigonal character of these sites, we have adopted the value $a_{int} \approx -15$ MHz obtained for the isotropic part of the **A**-tensor of Power's trigonal planar complex.[5] Since the terminal site has tetrahedral sulfur coordination, we use $a_{int} = -22$ MHz.[68] Substitution yields $\langle A_1\rangle_{av} = -15$ MHz, $\langle A_2\rangle_{av} = +12$ MHz, and $A_3 = -7$ MHz, in excellent agreement with the experimental values. In the present analysis, the magnetically unique site A_3 coincides with the structurally exceptional site, Fe_T, which is aesthetically more appealing than having a unique site among six similar equatorial sites. We are cognizant that the relative strengths of the exchange interactions in the cofactor may not warrant any rigorous hierarchy in the coupling of the spins. However, the following considerations lend support to the electronic structure in Figure 2. Substantial delocalization in the triangles is consistent with the observation that all iron sites of M^N have the same ΔE_Q. Electron delocalization results from interatomic resonance interactions, described by the electron-transfer parameter β. Given that the transfer parameter is positive in the cuboidal $d^5d^5d^6$ cluster $[Fe_3S_4]^0$,[69] β is likely negative for hole transfer in the $d^5d^6d^6$ triangles of the cofactor. For $\beta < 0$, the resonance interaction results in a fully delocalized, spin-ordered state, $^{14}A_1$. This state is the ground state of the triangle, provided the antiferromagnetic exchange interactions between the Fe sites are sufficiently weak so as to prevent the stabilization of a state with lower spin. This requirement may be fulfilled for the predominantly ferrous Fe_{Eq} sites between which the antiferromagnetic couplings are anticipated to be weaker than those between ferric sites.[6,23] The canting of S_3 relative to S_2 may be due to a combination of double exchange, arising from incipient electron delocalization toward the terminal site, and regular antiferromagnetic exchange interactions.[70] A quantitative comparison of the spin-ordering energy of Figure 2 with that of alternative patterns is a subject of future research.

The value for a_{int} in Power's trigonal complex,[5] -15 MHz, is ca. 30% smaller than that of a rubredoxin-type FeS_4 site. The reduction correlates with a shorter Fe$-$S distance, 2.27 vs 2.32 Å, respectively. The successful application of the trigonal a_{int} value to M^N supports the notion that the bonding interactions between the interstitial atom and the equatorial irons are weak. This idea is further corroborated by the short $Fe_{Eq}-S$ distance of 2.26 Å, which is, within the error margin, equal to the corresponding bond distance in Power's trigonal complex.

3.2. Redox-Structural Correlations. 3.2.1. Cluster Contraction. The calculated Fe$-$X distances in Table 4 shorten upon reduction of the cluster (Figure 3), except for an irregularity for [4Fe^{2+}3Fe^{3+}:O]. This trend is remarkable

(68) Yoo, S. J.; Meyer, J.; Achim, C.; Peterson, J.; Hendrich, M. P.; Münck, E. *J. Biol. Inorg. Chem.* **2000**, *5*, 475.
(69) Borshch, S. A.; Bominaar, E. L.; Blondin, G.; Girerd, J. J. *J. Am. Chem. Soc.* **1993**, *115*, 5155.
(70) While it is difficult to assign reliable δ values to individual Fe sites, Yoo et al.[2] have pointed out that none of the sites can have $\delta < 0.34$ mm s^{-1}, suggesting for Fe_T the isomer shift appropriate for a ferric tetrahedral site, $\delta = 0.25$ mm s^{-1}, has increased by some delocalization from the equatorial sites. Such delocalization may also reduce a_{int} of this site and improve the match with the experimental data.

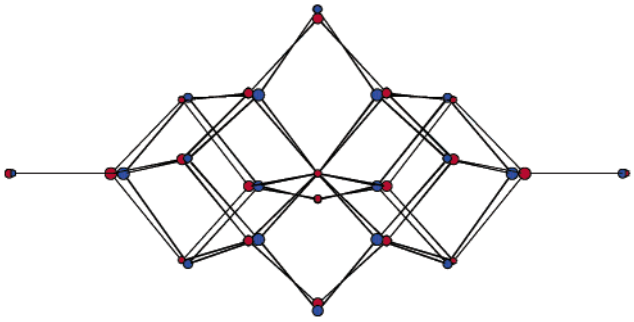

Figure 3. Overlay of optimized B3LYP/6-311G structures, which shows reduction-induced contraction of iron frame: red, $[0Fe^{2+}8Fe^{3+}:N]$; blue, $[4Fe^{2+}4Fe^{3+}:N]$.

Table 9. Contraction of Average Fe−Fe Distance with Reduction State

X	oxidation state[a]	$(FeFe)_{av}$[b] (Å)	$-\Delta(FeFe)_{av}$/electron (Å)
C	$[0Fe^{2+}8Fe^{3+}]$	3.120	0.031
	$[4Fe^{2+}4Fe^{3+}]$	2.998	
N	$[0Fe^{2+}8Fe^{3+}]$	3.153	0.038
	$[4Fe^{2+}4Fe^{3+}]$	3.003	
O	$[0Fe^{2+}8Fe^{3+}]$	3.313	0.029
	$[4Fe^{2+}4Fe^{3+}]$	3.200	
FeMoco	M^N	2.58	0.04[c]
	M^R	2.54	

[a] Of model cluster used for calculating distances, see Table 4. [b] Averages based on expression, eq 1, for $[7Fe^{3+}]$ and $[4Fe^{2+}3Fe^{3+}]$. [c] Contraction in average of nearest FeFe distances upon one electron reduction, observed by EXAFS measurements by Cramer and co-workers.[7]

because metal−ligand bonds usually lengthen by adding electrons. Apparently, the Fe_{Eq}−X distance is not the result of coordinative interactions between the Fe_{Eq} sites and X, despite distances that are characteristic for coordination bonds, but is controlled by the interactions between the peripheral irons and sulfurs. This conclusion is consistent with the small δ changes per added electron (see above) and a high number of weak Fe_{Eq}−X interactions. The reduction-induced shortening of Fe_{Eq}−X is accompanied by a contraction of the Fe_{Eq}−Fe_{Eq} (and Fe_{Eq}−Fe_T) distances (Table 4). The contraction is confirmed by EXAFS results on M^N and the one-electron oxidized state of FeMoco, M^{OX},[7] and amounts to a decrease of 0.04 Å in the mean values of the nearest Fe−Fe distances for the two states (Table 9). Calculated estimates of the mean Fe−Fe distances, obtained by substituting the geometry-optimized distances of Table 4 into the expression for the averaged Fe−Fe distance in an idealized, molybdenum-substituted cluster

$$(FeFe)_{av} = \frac{1}{24}[6(Fe_TFe_{Eq}) + 12(Fe_{Eq}Fe_{Eq'}) + 6(Fe_{Eq}Fe_{Eq})] \quad (1)$$

are also listed in Table 9 and used to predict the contraction per added electron (last column). The calculated contractions depend slightly on the choice for interstitial X and are all in reasonable agreement with the EXAFS value.[7] Although the best agreement is obtained for X = N, supporting the notion of a central nitride, the differences with the contractions for the other elements are marginal and therefore inconclusive.

Table 7 presents Mulliken charges and bond angles as a function of formal oxidation state for the carbide, nitride, and oxide models. As already noted in earlier studies of mononuclear FeS_4 sites,[35,71−75] the addition of electrons enhances the sulfur (and chloride) charges but has a comparatively small effect on the iron charges. For example, the $4e^-$ reduction of $[0Fe^{2+}7Fe^{3+}:X]$ to $[4Fe^{2+}3Fe^{3+}:X]$ changes the charges of S_{Eq}, S_T, and Cl by, respectively, −0.40, −0.27, and −0.35 (X = C), −0.37, −0.26, and −0.41 (N), and −0.49, −0.26, and −0.40 (O). The charging of the ligand bridges correlates with changes in the bond angles at S_{Eq} (Table 4, third column) and in the summed angles at S_T (i.e., $Fe_{Eq}S_TFe_{Eq'} + 2 \times Fe_TS_TFe_{Eq}$); the angular changes between $[0Fe^{2+}7Fe^{3+}:X]$ and $[4Fe^{2+}3Fe^{3+}:X]$ are −14.5°, −10.9° (C), −15.5°, −11.6° (N), and −9.7°, −10.0° (O). The correlation suggests that the iron−sulfur−iron bond angles become more acute as a result of an increase in the electron-pair repulsions between the sulfur lone pairs and the electrons in the iron−sulfur bonds. This possibility is discussed in section 3.2.2. The Mulliken charges of interstitial atoms X are less negative than their formal charge. The interstitial atoms in the $[0Fe^{2+}7Fe^{3+}:X]$ states donate the charges −1.65 (C^{4-}), −1.29 (N^{3-}), and −0.80 (O^{2-}) to the peripheral atoms of the cluster. As expected, electron donation from X decreases in the more reduced states, but does so by only a small amount (∼0.1e^- for $4e^-$ reduction). The reduction-induced decrease of the $Fe_{Eq}S_{Eq}Fe_{Eq}$ angles correlate with a decrease in the ratio $Fe_{Eq}X$:$S_{Eq}X$. For example, in the case of the equatorial atoms in $[nFe^{2+}(7 - n)Fe^{3+}:N]$, the ratios are 0.66 ($n = 0$), 0.61 ($n = 2$), 0.59 ($n = 4$), and 0.57 ($n = 6$). These changes can by brought about by either outward sulfur displacements or inward iron displacements.

The data in the sixth and seventh columns of Table 4 indicate that the changes in the $Fe_{Eq}S_{Eq}Fe_{Eq}$ angles originate equally from inward Fe_{Eq} motions and outward S_{Eq} motions. Similar results were obtained for the cuboidal cofactor moieties on the basis of the Fe−Fe' and S−S' distances therein (not presented here). This analysis does not support resonance interactions of the double-exchange type between the spin parallel aligned equatorial irons of the theoretical model as a possible cause of the shortening of the intermetal distances in the geometry-optimized structures because the contraction persists in the reduced states $[4Fe^{2+}3Fe^{3+}:X]$ and $[6Fe^{2+}1Fe^{3+}:X]$ in which the central irons have lost, to a major extent, their mixed-valence character due to the preponderance of metals with formal d^6 configurations. The antiparallel spin ordering in the actual cofactor allows, in principle, for a shortening of the iron separations by the formation of Heitler−London bonds between the metal ions. However, the observed manifestation of incipient metal−metal bond formation, namely, the antiferromagnetic exchange parameter $J(Fe^{3+}-Fe^{3+}) < 300$ cm^{-1} in $JS_i \cdot S_j$ in cubanes,[76] is weaker than that obtained from broken spin

(71) Norman, J. G., Jr.; Jackels, S. C. *J. Am. Chem. Soc.* **1975**, *97*, 3833.
(72) Noodleman, L.; Norman, J. G., Jr.; Osborne, J. H.; Aizman, A.; Case, D. A. *J. Am. Chem. Soc.* **1985**, *107*, 3418.
(73) Kennepohl, P.; Solomon, E. I. *Inorg. Chem.* **2003**, *42*, 696.
(74) Kennepohl, P.; Solomon, E. I. *Inorg. Chem.* **2003**, *42*, 689.
(75) Kennepohl, P.; Solomon, E. I. *Inorg. Chem.* **2003**, *42*, 679.

Table 10. Results for $[Fe_4S_4Cl_4]^n$, $n = 0, ..., -4$[a]

property	$n = 0$	$n = -1$	$n = -2$	$n = -3$	$n = -4$
(d-AO) β MOs		B_1	EE	B_1EE	B_1A_2EE
Fe−S−Fe (deg)	90.5	89.5	89.4	88.1	86.2
S−Fe−S (deg)	90.6	90.9	90.2	90.7	92.5
X−Fe (Å)	2.123	2.111	2.149	2.127	2.122
X−S (Å)	2.103	2.114	2.155	2.196	2.264
X−Fe/X−S	1.010	0.999	0.997	0.969	0.937
Q(Fe) (au)	1.271	1.263	1.282	1.238	1.231
Q(S) (au)	−0.875	−0.969	−1.084	−1.215	−1.362
Q(Cl) (au)	−0.397	−0.544	−0.698	−0.773	−0.869
Fe···Fe (Å)	3.467	3.435	3.509	3.554	3.492
S···S (Å)	3.433	3.489	3.519	3.602	3.655
Fe−S (Å)	2.440	2.448	2.477	2.532	2.531
Fe−Cl (Å)	2.173	2.223	2.359	2.381	2.548
δ (mm s^{-1})	0.396	0.496	0.583	0.709	0.845

[a] Calculated with B3LYP/6-311G in ferromagnetic state; geometry D_{2d} close to T_d.

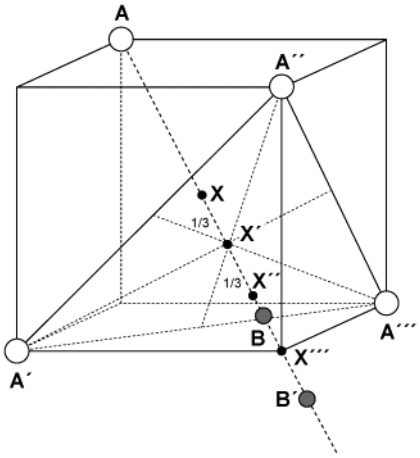

Figure 4. Position of a B atom relative to A atoms in [4A−4B] cluster, consisting of the intercalated tetrahedra spanned by atoms A and B (see text for further details).

symmetry calculations[77] and may therefore have less influence on the intermetallic separations than originally anticipated.

3.2.2. Redox-Structural Correlations in Cuboidal Clusters. To investigate whether the "redox-structural correlation" between the oxidation state and metal−metal separations is a cofactor specific feature rather than a more general property of iron−sulfur clusters, we have performed DFT calculations for five formal oxidation states of the cuboidal cluster $[Fe_4S_4Cl_4]^n$ [53,78,79] (Table 10). Table 10 reveals the existence of similar correlations as to the cofactor model between the redox state and the following parameters: angle FeSFe, ratio FeX:SX and the charges of the irons, sulfurs, and chlorides (FeX and SX are the distances of the irons and the sulfides to the center of gravity, X, of the cluster; see Figure 4). However, contrary to the case of the cofactor, the decrease in the ratio FeX:SX upon reduction of cubanes is due to an expansion of the S−X distances at nearly constant Fe−X. As a consequence, the Fe−Fe distances are nearly constant, while the S−S distances increase. The Fe−Fe distances deviate only slightly from the averaged separation, 3.445 Å, taken over the distances for the five oxidation states, with a mean deviation modulus of 0.028 Å. The S−S distances have an average of 3.547 Å and increase by about 0.055 Å per added electron.

Figure 4 illustrates the two principal ways in which a decrease of the iron−sulfur−iron angles can be realized. First, we assume that the vertices labeled with A and B represent spatially fixed irons and a movable sulfur, respectively, that belong to the intercalated tetrahedra of a symmetrized [4Fe−4S] cubane. The special points indicated in the figure are defined as follows. X is the gravity center, X′ is the intersection of diagonal AX‴ and the plane (A′A″A‴), X″ is located on AX‴ at the same distance as X from this plane, and X‴ is a vacant site of the cube spanned by the atoms labeled with an A. The angle A′YA″ is equal to $\theta_t \approx 109.5°$, 120°, θ_t, and 90° for Y = X, X′, X″, and X‴, respectively. Thus, if sulfur atom B′ is positioned in the segment XX′, a decrease of the iron−sulfur−iron angle A′B′A″ corresponds to an inward motion of B′, while if B′ is outward of X′, the same angular change requires an outward motion of B′. The sulfurs in [4Fe−4S] clusters are located outward from X‴ (A′B′A″ ≈ 73−75°) so that a decrease of the iron−sulfur−iron angle can be realized by outward displacement of the sulfur. Second, if the A vertices represent spatially fixed sulfur atoms and B is a movable iron atom that is located between X″ and X‴, like the irons in [4Fe−4S] clusters (A′BA″ ≈ 103−105°), then a decrease of the iron−sulfur−iron angle would require inward motion of iron B. The calculations indicate that the decrease of the bridging sulfur angles in the optimized geometries of $[Fe_4S_4Cl_4]^n$ as a function of increasing magnitude of n is realized by an outward motion of the sulfurs. This prediction has been tested against experimental results. Crystallographic structure data for $[Fe_4S_4R_4]$ units in oxidation states corresponding to the $n = -1$, -2, and -3 states of the tetrachloride cluster have been reviewed by Berg and Holm (Table 7 of ref 80). A comparison with the computational results reveals that the average S−S distances come out about right (3.613 vs 3.547 Å), while the Fe−Fe distance are systematically too long (2.73 vs 3.445 Å). The redox-structural correlations observed in [4Fe−4S] cubanes are in excellent agreement with the trends deduced from the computational results. Thus, the crystallographic Fe−Fe distances are almost constant, with a mean deviation of 0.009 Å from the average distance 2.73 Å, and the S−S distances increase by 0.051 Å per added electron. This trend is confirmed by the crystal structure of the all-ferrous $[Fe_4S_4]^0$ form of the nitrogenase iron protein, although the decrease of the sulfide bond angles therein is accompanied by a slight inward iron displacement.[81] The reduction-induced displacements of the central six Fe_{Eq} of the cofactor model reflect the increase in iron mobility afforded by the quasi 3-fold

(76) Yoo, S. J.; Hu, Z.; Goh, C.; Bominaar, E. L.; Holm, R. H.; Münck, E. *J. Am. Chem. Soc.* **1997**, *119*, 8732.
(77) Noodleman, L.; Case, D. A. *Adv. Inorg. Chem.* **1992**, *38*, 423.
(78) Kanatzidis, M. G.; Baenziger, N. C.; Coucouvanis, D.; Simopoulos, A.; Kostikas, A. *J. Am. Chem. Soc.* **1984**, *106*, 4500.
(79) Trautwein, A. X.; Bill, E.; Bominaar, E. L.; Winkler, H. *Struct. Bonding* (*Berlin*) **1991**, *78*, 1.
(80) Berg, J. M.; Holm, R. H. In *Metal Ions in Biology*; Spiro, T. G., Ed.; Wiley: New York, 1982; Vol. 4, p 1.
(81) Strop, P.; Takahara, P. M.; Chiu, H.-J.; Angove, H. C.; Burgess, B. K.; Rees, D. C. *Biochemistry* **2001**, *40*, 651.

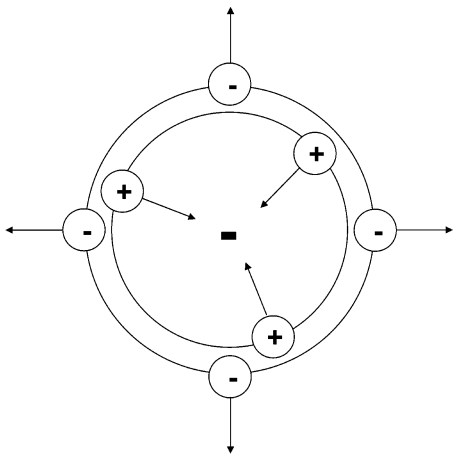

Figure 5. A two-dimensional example of charged-sphere model for rationalizing the redox-structural correlations in Fe−S clusters. There are four atoms with a negative unit charge and three atoms with a positive unit charge. Together they yield the effective charge $Z_{eff} = -1$. Equal distribution of Z_{eff} over a sphere gives rise to a monopolar Coulomb potential that can be generated by placing a virtual charge of size Z_{eff} in the center. The resulting Coulomb forces on the charged atoms are indicated by arrows.

coordinations in the cofactor relative to the spatially restraining 4-fold coordinations prevailing in cubanes. The success of DFT in predicting the redox-structural correlations prevailing in the well-characterized set of cuboidal clusters supports the use of the ferromagnetic state in structure calculations, vindicates its application to the cofactor, and corroborates the conclusion that the cofactor contracts upon reduction. The approach is also supported by the most recent computations on [4Fe−4S] clusters, where geometry optimizations in both broken symmetry and ferromagnetic states yielded nearly identical structures.[82]

To test whether a lone-pair repulsion mechanism can explain the redox-structural correlations (section 3.2.1), we have performed B3LYP/6-311G geometry optimizations for the cuboidal oxygen and nitrogen analogues $[Fe_4O_4Cl_4]^n$ and $[Fe_4(NH)_4Cl_4]^n$,[83] $n = 0, -1, ..., -4$ (data not shown). Interestingly, these calculations reveal the existence of a similar dependency of the structure on the cluster oxidation state but without there being any significant accompanying changes in the Mulliken charges of the oxide bridges. This result conflicts with the notion of lone-pair repulsion as the major cause of the redox-structural correlations in the bridging ligand angles and points toward a general mechanism based on the electrostatic interactions in the clusters.

The total cluster charge is neutral in the most oxidized state and becomes increasingly more negative upon reduction. If we consider the cluster as a charged sphere, the potential at the surface, i.e., where the atoms are located, is the potential generated by a point charge at the center with charge equal to the total charge of the cluster, n (Figure 5). As a consequence, atoms carrying the majority charge (negative charge if $n < 0$ and vice versa) are subjected to an outward-directed force and atoms carrying a minority

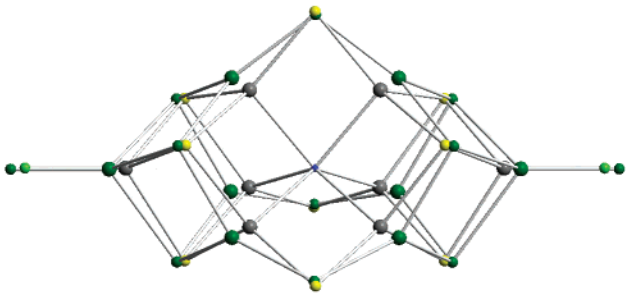

Figure 6. Overlay of optimized B3LYP/6-311G structures, which shows the effect of the interstitial ion N^{3-} on the positions of the metal centers: green, $[Ga_8S_9Cl_2]^{4+}$; gray, $[Ga_8S_9Cl_2N]^{1+}$; blue, N; yellow, S.

charge (positive charge if $n < 0$) to an inward-directed force. In the case $n \leq 0$, as found in iron−sulfur clusters, electron addition increases both the inward forces on the positively charged irons and the outward forces on the negatively charged ligand bridges (Figure 5) and leads to the observed trends in the data for S−X distances and FeSFe angles listed in Table 10.

A similar correlation exists in the cofactor, as can be seen from the relationship between cluster charge (second column of Table 4) and $Fe_{Eq}X$ (sixth column) and $S_{Eq}X$ (seventh column). Along the same line of argument, a negatively charged interstitial ion in the center of the cluster pulls the positively charged metal ions inward. Figure 6 illustrates the effect of an interstitial nitride on the positions of the gallium atoms in the B3LYP/6-311G optimized structures of $[Ga_8S_9Cl_2]^{4+}$ and $[Ga_8NS_9Cl_2]^{+}$.[84] The displacements of the equatorial metal sites under the influence of X are not strictly directed along the normal of the MS_3 planes and thus give rise to EFGs with large asymmetry parameters, $\eta \sim 1$ (see below). The geometry optimizations for the empty cluster $[Fe_8S_9Cl_2]^n$ reveal the same redox-structural correlations as in the presence of X. However, in the absence of the central force exerted by X, the Fe_{Eq} atoms remain at the exterior side of the trigonal coordination planes, even in the all-ferrous state. The force constant for the "out-of-plane" coordinate of a trigonal planar Fe^{2+} is estimated by DFT to be 2×10^5 cm^{-1}/Å^2 for $[FeCl_3]^-$ and yields a displacement of 0.7 Å under the influence of the Coulomb force exerted by an apical X^- ion located at 2.7 Å from Fe. We are aware that the out-of-plane distortions depend also on the rigidity of the $M^{n+}S_3$ planes. Since the rigidity may change with redox state and with the number of electrons donated by X this factor will likely introduce additional complexities in the interpretation of the redox-structural correlations.[85] Finally, as a corollary, a negative net charge ($-1, ..., -3$) on a cuboidal Fe−S cluster enhances the stability of a structure in which small Fe spheres are packed inside a tetrahedron of large sulfur spheres. Significant deviations from the aforementioned charge range lead to serious SCF convergence problems even for closed-shell systems that are known to mimic Fe^{2+} and Fe^{3+} ions in geometry optimization (e.g., $[Ga_8S_9Cl_2]^{4+}$ and $[Zn_8NS_9Cl_2]^{7-}$, which model the all-

(82) Torres, R. A.; Lovell, T.; Noodleman, L.; Case, D. A. *J. Am. Chem. Soc.* **2003**, *125*, 1923.
(83) Duncan, J. S.; Nazif, T. M.; Verma, A. K.; Lee, S. C. *Inorg. Chem.* **2003**, *42*, 1211.
(84) On the basis of its size and charge, the diamagnetic ion Ga^{3+} is a suitable substitute for high-spin Fe^{3+} in geometry optimizations.
(85) Bominaar, E. L.; Block, R. *J. Chem. Phys.* **1991**, *95*, 6712.

oxidized $[Fe_8S_9Cl_2]$ and all-reduced $[Fe_8NS_9Cl_2]$, respectively). However, tight convergence of the wave function can be attained by replacing X by a negative point charge, Q. Geometry optimized structures for $[Ga_8S_9Cl_2]^{4+}/Q = -4$, -2, and -1 exhibit Ga−Q distances of 1.205, 1.655, and 2.014 Å, corroborating the Coulombic nature of the interaction between atom X and the equatorial irons. The $Q = -1$ calculations show the closest overall structure similarity with $[Ga_8NS_9Cl_2]^+$ and along with Mulliken population analysis (see above) suggest that the nitride ion donates approximatively two electrons to the cluster.

3.3. Concluding Remarks. In summary, this study has answered some of the questions posed in the Introduction. The likelihood that the interstitial atom X is one of the following atoms decreases in the order N > C > O. Atom X is present not only in M^N but also in M^{OX}, in M^R, and in the resting states of the alternative nitrogenases [FeVco] and [FeFeco]. X is negatively charged and pulls the equatorial irons inward, leading to a contraction of the average Fe−Fe distance upon reduction of the cofactor. The Fe−X interactions have an ionic rather than a covalent character and perturb the electronic states of the irons only slightly. The interstitial atom raises the values of the isomer shifts of the equatorial iron sites and affects the EFG asymmetry parameter, η, by pulling them out of the trigonal S_3 coordination planes along directions that do not coincide with the normals of these planes. The formal oxidation state of M^N is $[Mo^{4+}\text{-}4Fe^{2+}3Fe^{3+}]$ rather than the state $[Mo^{4+}6Fe^{2+}1Fe^{3+}]$ proposed in previous studies.

The presence of nonbonding Fe_{Eq}−X distances in the higher oxidation states of the cofactor model, e.g., 2.326 Å in $[0Fe^{2+}7Fe^{3+}{:}N]$, raises the possibility that the central atom in FeMoco is the remnant of the catalytic cycle rather than a structural element. Although this possibility is consistent with the empirical and computational data for the isomer shift, ENDOR studies do not support an exchange of interstitial N in the catalytic cycle.[86] Moreover, the retention of X in M^{OX} and M^R, inferred from δ_{av} (section 3.1.8), supports the notion of X being a permanent element of the cofactor. The quasi-trigonal character of the equatorial irons deduced from the hyperfine interactions suggests that these sites may retain considerable reactivity in the presence of the interstitial atom. Further work will be required to elucidate the role of the central atom.

Note Added in Proof. Lovell et al. have just reported DFT calculations that yielded for FeMoco, based on a previous calibration, $\delta_{av} = 0.54$ mm s^{-1} for $[6Fe^{2+}1Fe^{3+}N^{3-}]$ and $\delta_{av} = 0.48$ mm s^{-1} for $[4Fe^{2+}3Fe^{3+}N^{3-}]$, while δ_{av} for $[2Fe^{2+}5Fe^{3+}N^{3-}]$ was not considered (Lovell, T.; Liu, T.; Case, D. A.; Noodleman, L. *J. Am. Chem. Soc.* **2003**, *125*, 8377). The authors suggest that a $[4Fe^{2+}3Fe^{3+}N^{3-}]$ assignment of M^N is more compatible with the experimental $\delta_{av} = 0.40$ mm s^{-1} than their previous $[6Fe^{2+}1Fe^{3+}]$ assignment.

Acknowledgment. We thank Dr. Robert Stewart from the Department of Chemistry, Carnegie Mellon University for a helpful discussion on X-ray crystallography. This research was supported by National Science Foundation Grant MCD 9416224 (E.M.).

Supporting Information Available: Correlation plot of δ_{exp} vs $\rho_{calc}(0)$ for the calibration set of iron compounds, and plot of B3LYP/6-311G-calculated isomer shift in the ferromagnetic state vs the total charge of the geometry-optimized cluster. This information is available free of charge via the Internet at http://pubs.acs.org.

IC0301371

(86) Lee, H.-I.; Benton, P. M. C.; Laryukhin, M.; Igarashi, R. Y.; Dean, D. R.; Seefeldt, L. C.; Hoffman, B. M. *J. Am. Chem. Soc.* **2003**, *125*, 5604.